Chinese Chemical Letters 36 (2025) 110392

Contents lists available at ScienceDirect

Chinese Chemical Letters

journal homepage: www.elsevier.com/locate/cclet

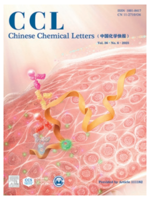

Advancements in MXene-based nanohybrids for electrochemical water splitting

Liwei Hou[a,b], Xianyun Peng[a,c,*], Siliu Lyu[e], Zhongjian Li[a,c], Bin Yang[a,c], Qinghua Zhang[a], Qinggang He[a], Lecheng Lei[a,c], Yang Hou[a,c,d,*]

[a] Key Laboratory of Biomass Chemical Engineering of Ministry of Education, College of Chemical and Biological Engineering, Zhejiang University, Hangzhou 310027, China
[b] College of Ocean Science and Engineering, Shanghai Maritime University, Shanghai 201306, China
[c] Institute of Zhejiang University - Quzhou, Quzhou 324000, China
[d] Zhejiang University Hydrogen Energy Institute, Hangzhou 310027, China
[e] Hubei Key Laboratory of Automotive Power Train and Electronic Control, School of Automotive Engineering, Hubei University of Automotive Technology, Shiyan 442002, China

ARTICLE INFO

Article history:
Received 14 July 2024
Revised 4 August 2024
Accepted 29 August 2024
Available online 31 August 2024

Keywords:
Two-dimensional MXene
Electrocatalytic
Water splitting
Hydrogen evolution reaction
Oxygen evolution reaction

ABSTRACT

Electrochemical water splitting presents a promising, environmentally friendly alternative to fossil fuels for hydrogen production. However, the efficiency is constrained by the sluggish kinetics and high overpotentials associated with the hydrogen evolution reaction (HER) and oxygen evolution reaction (OER). While noble metal catalysts, such as Pt for HER and Ir for OER, currently offer superior performance, their widespread adoption is hindered by high cost and scarcity. This has spurred research into cost-effective alternatives, with a focus on understanding the underlying electrocatalytic mechanisms. MXenes, a class of two-dimensional materials, have emerged as promising candidates for electrocatalytic water splitting due to their unique physical and chemical properties. However, research in this field remains largely experimental, lacking a comprehensive understanding of fundamental mechanisms. This knowledge gap impedes the development of high-efficiency electrocatalysts and necessitates further investigation. This review systematically examines recent advancements in MXene-based nanohybrids for electrocatalytic water splitting, covering synthetic methods, structure-property relationships, and performance enhancement strategies. It encompasses both precious and non-noble metal-based systems for HER, OER, and overall water splitting applications. Additionally, this review addresses current challenges, opportunities, and future research directions for MXene-based nanohybrids. By providing comprehensive insights into the development of high-performance MXene-based electrocatalysts, this review aims to accelerate progress in the field of electrochemical water splitting. It serves as a valuable resource for researchers and engineers working towards more efficient and sustainable hydrogen production technologies, potentially contributing to the broader goal of transitioning away from fossil fuels towards cleaner energy sources.

1. Introduction

Hydrogen fuel represents a promising avenue towards clean, abundant, renewable, and highly efficient energy generation, distinguished by its exceptional calorific value of 142.351 kJ/kg and the fact that its sole combustion by-product is environmentally benign water, thereby mitigating pollution concerns [1-4]. However, most hydrogen is produced by steam reforming from fossil fuel sources. This production route consumes fossil fuels and suffers from low conversion rates and greenhouse gas emissions [1,5-9]. Green hydrogen, produced by water electrolysis using renewable energy sources, is increasingly being recognized as a key player in environmental and economic sustainability. Compared to these traditional hydrogen production technologies, electrocatalytic water splitting is an environmentally friendly hydrogen production technology that utilizes widely available water as its primary raw material [10-12]. Electrocatalytic water splitting involves two half-reactions: Hydrogen evolution reaction (HER) and oxygen evolution reaction (OER) [13]. Noble metals (*e.g.*, Pt, Ru, and Ir) and their oxides (*e.g.*, RuO_2 and IrO_2) are widely used as electrocatalytic water-cracking catalysts owing to their high activity and stability; however, their scarcity and high cost have hindered their large-scale

---

[*] Corresponding authors.
E-mail addresses: xianyunpeng@zju.edu.cn (X. Peng), yhou@zju.edu.cn (Y. Hou).

https://doi.org/10.1016/j.cclet.2024.110392

application in industry and daily life [14-20]. In addition, it is difficult for single precious-metal-based catalysts to maintain high performance in an identical electrolyte solution. Therefore, developing cost-effective catalysts and studying the corresponding mechanisms of electrocatalytic water splitting is economically and practically valuable.

Two-dimensional (2D) materials, particularly MXenes, have emerged as promising candidates for electrocatalysis due to their unique electronic and structural properties [21]. MXenes, a family of 2D transition metal carbides, nitrides, and carbon-nitrides, stand out among other 2D materials for their excellent electrical conductivity, favorable hydrophilicity, tunable physical and chemical structures, and distinctive micro-ceramic architecture [22-24]. Compared with other 2D materials, MXene is considered the next promising electrocatalytic candidate owing to its excellent electrical conductivity, favorable hydrophilicity, extremely rich and controllable physical phase structure and surface chemistry, and unique microceramic structure. MXene can be used as both catalysts and carriers. However, most MXenes lack catalytically active structures suitable for electrocatalysis and thus show unsatisfactory catalytic activity [25-28]. The electrocatalytic activity of MXene and MXene-based materials can be enhanced by various nanostructural and catalytic center design strategies, including terminal engineering, heteroatom doping, and defect engineering [29]. In addition, MXene exhibits excellent corrosion resistance, hydrophilicity, and good electrochemical stability under redox conditions compared with carbon-based carriers [30,31]. When used as a support, the abundant functional groups on the surface of MXene can effectively avoid the aggregation of nanomaterials, and their metal-support interactions can also stabilize the active metal and modulate the catalytic activity of multiphase water decomposition. Therefore, MXenes show great promise as electrocatalysts and supports for electrochemical water splitting [32-36]. Ongoing research continues to unlock the full potential of MXenes in advancing sustainable energy technologies, with a focus on optimizing their catalytic centers and leveraging their unique properties as support materials for high-performance electrocatalysts.

In this review, we provide a comprehensive overview of MXene-based nanohybrids for electrochemical water splitting, as summarized in Table 1 [37-68]. We focus on the significant advancements made over the past five years in both precious and non-noble metal-based MXenes for HER, OER, and overall water splitting processes. Our analysis encompasses the underlying reaction mechanisms of HER and OER, the catalytic mechanisms exhibited by MXenes, their performance characteristics, and the diverse synthesis methods employed to create these innovative materials. By examining these aspects, we aim to elucidate the potential of MXenes as high-performance electrocatalysts for water splitting. Our ultimate goal is to contribute to the development of MXene-based catalysts that can effectively replace precious metal-based alternatives, thereby promoting the widespread adoption of electrocatalytic water splitting technologies. This review serves as a valuable resource for researchers and engineers working towards more efficient and sustainable hydrogen production methods, potentially accelerating the transition to clean energy systems.

2. HER and OER mechanisms

2.1. HER mechanisms

The HER, the cathodic half-reaction in water electrolysis, involves the reduction of protons (H^+) or water molecules (H_2O) to generate H_2, which is a fundamental electrochemical process central to many energy conversion technologies, functioning as a two-electron transfer mechanism [69]. This reaction exhibits distinct pathways depending on the electrolyte pH and the electrode surface conditions. In acidic environments, HER is initiated by the Volmer reaction, where hydronium ions are discharged at the electrode surface, forming adsorbed hydrogen intermediates (H^*): $H_3O^+ + e^- + {}^* \rightarrow H^* + H_2O$. Conversely, in alkaline media, water molecules serve as the proton source: $H_2O + e^- + {}^* \rightarrow H^* + OH^-$. The subsequent formation of molecular hydrogen occurs *via* two competing routes that are largely determined by the surface coverage of H^*. When the H^* coverage is high, the Tafel step becomes rate-limiting, involving the combination of two adjacent H^* atoms to form H_2: $H^* + H^* \rightarrow H_2$. This step is often considered the determining factor in the overall reaction kinetics under such conditions. In contrast, a low H^* coverage favors the Heyrovský reaction, where a single H^* interacts with an additional proton and an electron. In acidic conditions, this manifests as: $H^* + H_3O^+ + e^- \rightarrow H_2 + H_2O$, while in alkaline environments, it proceeds as: $H^* + H_2O + e^- \rightarrow H_2 + OH^-$. The dominance of either the Tafel or the Heyrovský mechanism significantly influences the reaction efficiency and rate, making understanding these pathways crucial for designing advanced electrocatalysts. Furthermore, the interplay between these mechanisms and the electronic structure of the electrode material, surface morphology, and catalytic properties plays a pivotal role in optimizing the HER performance across various pH ranges and operational conditions.

The free energy of hydrogen adsorption (ΔG_{H^*}) is a crucial parameter that influences the hydrogen evolution kinetics of catalysts. An ideal catalyst, such as Pt, exhibits a ΔG_{H^*} value close to zero. This optimal value ensures a balance between the adsorption and desorption processes. When the adsorption is too weak, there is insufficient interaction between the protons and electrode surface, leading to suboptimal performance. Conversely, a large ΔG_{H^*} value implies strong bonding between hydrogen and the catalyst surface, making it difficult for H_2 to desorb, which impedes the overall reaction kinetics.

By plotting the experimentally determined exchange current densities for a variety of catalysts against their corresponding ΔG_{H^*} values calculated using density functional theory (DFT), researchers can observe a volcano-shaped relationship [70]. This relationship clearly illustrates the HER activity of different metals. The peak of this volcano diagram represents the ideal catalyst with the highest activity, whereas the other points on the curve indicate varying degrees of efficiency based on how closely their ΔG_{H^*} values approach zero. This visual representation through volcano diagrams offers a clear method for comparing the reactivity of different metals. It guides material design by highlighting the relative performance of catalysts with respect to the binding energies of the reactive intermediates on their surfaces. Consequently, it aids in identifying promising candidates for improving HER catalysts and optimizing their surface properties to enhance electrocatalytic efficiency.

2.2. OER mechanisms

The OER, which is the anodic half-reaction in water electrolysis, is more complex and energetically demanding than the HER. This process involves the oxidation of water molecules to produce O_2. The OER is a crucial yet kinetically challenging process in electrochemical water splitting and plays a pivotal role in various renewable energy technologies. Characterized as a sluggish four-electron transfer process, the OER involves the formation and transformation of three key surface-adsorbed intermediates: OOH^*, O^*, and OH^* [71]. This complexity contributes to its significant overpotential requirement and underscores the importance of developing efficient catalysts to overcome these kinetic barriers. The reaction mechanism of the OER involves pH-dependent pathways. In acidic environments, water molecules serve as the primary reactants, undergoing oxidation to produce oxygen and hydrogen ions.

Table 1
Summary of electrochemical performance of MXene-based nanohybrids for water splitting.

Catalysts	Electrolyte	Application	η_{10} (mV)	Tafel slope (mV/dec)	Voltage of water splitting (V)	Ref.
d-Ti_3C_2/V_2O_5	1.0 mol/L KOH	HER	90	49	–	[37]
Pt/MXene	1.0 mol/L KOH	HER	34	29.7	–	[38]
E-$Ti_3C_2T_x$	0.5 mol/L H_2SO_4	HER	190	60.7	–	[39]
CSEXM	0.5 mol/L H_2SO_4	HER	230	65	–	[40]
$Ti_3C_2T_x$@ZIF-8	1.0 mol/L KOH	HER	507	77	–	[41]
CPN@TC	1.0 mol/L KOH	HER	286	78	–	[42]
3%Rh/Ru-FeOOH@$Ti_3C_2T_x$	1.0 mol/L KOH	OER	306	63.6	–	[43]
$RuSnO_x$	0.1 mol/L $HClO_4$	OER	184	44.4	–	[44]
NiMX/NF	1.0 mol/L KOH	OER	245	191	–	[45]
MXene/NiFeP_x-NC	1.0 mol/L KOH	OER	240	81.2	–	[46]
NCMX	1.0 mol/L KOH	OER	220	94	–	[47]
MX@MOF-Co_2P	1.0 mol/L KOH	OER	246	28.18	–	[48]
NCSe@MGA	1.0 mol/L KOH	HER	78	55	–	[49]
		OER	201	79	–	
Co_8FS_8 MXene/NF	1.0 mol/L KOH	HER	108	84.08	1.51	[50]
		OER	171	24.97		
RuCo $Ti_3C_2T_x$	0.5 mol/L H_2SO_4	HER	60	34.8	1.56	[51]
	1.0 mol/L KOH	HER	52	38.7		
	1.0 mol/L KOH	OER	266	111.1		
Ru-RuO_2/MXene@CC	1.0 mol/L KOH	HER	43	52.1	–	[52]
Pt NPs/d-$Mo_2Ti_2C_3T_x$	1.0 mol/L $HClO_4$	HER	123@η_{100}	30.1	–	[53]
1T/2H $MoSe_2$/MXene	1.0 mol/L KOH	HER	95	91	1.64	[54]
MoS_2-Ti_3C_2 MXene	0.5 mol/L H_2SO_4	HER	98	45	–	[55]
CoNi-MOFNs@MX	1.0 mol/L KOH	OER	346	59.2	–	[56]
CoNi-$Ti_3C_2T_x$	1.0 mol/L KOH	HER	31	33	–	[57]
		OER	241	79.8	–	
Ru_{SA}-RuO_2/MXene@CC	0.5 mol/L H_2SO_4	HER	76	90	–	[58]
NiFeCo-LDH@MXene	1.0 mol/L KOH	HER	61	52	1.41	[59]
		OER	220	62		
CoS_2@MXene	0.1 mol/L KOH	HER	175	97	1.63	[60]
		OER	270	92		
Rh-SA/$Ti_3C_2O_x$	0.1 mol/L H_2SO_4	HER	23	27.8	–	[61]
	1.0 mol/L PBS	HER	85	77.4		
	0.1 mol/L KOH	HER	29	46.7		
Pt-SA/MXene	1.0 mol/L KOH	HER	33	43.9	–	[62]
$Ti_3C_2T_x$-Pt_{SA}	0.5 mol/L H_2SO_4	HER	38	45	–	[63]
Ir_{SA}-2NS-$Ti_3C_2T_x$	0.5 mol/L H_2SO_4	HER	57.7	25	–	[64]
	1.0 mol/L KOH	HER	40.9	50.5	–	
NiMX/NF	1.0 mol/L KOH	OER	245@η_{100}	191	–	[65]
MXene/NiFeP_x-NC	1.0 mol/L KOH	OER	240	81.2	–	[66]
Ni/Cr_2CO_2 MXene	1.0 mol/L KOH	HER	160	–	–	[67]
		OER	460	–	–	
Ru-SA/$Ti_3C_2T_x$	0.1 mol/L $HClO_4$	HER	70	27.7	1.56	[68]
		OER	290	37.9		

Note: η_x is the overpotential at a current density of $-x$ mA/cm^2 for HER or x mA/cm^2 for OER.

Conversely, in neutral and alkaline media, hydroxyl ions are oxidized, yielding water and oxygen. Theoretical models propose that, despite these different overall reactions, the OER proceeds through similar intermediate steps under both acidic and alkaline conditions. The generally accepted mechanism involves four consecutive proton-coupled electron transfer (PCET) steps. The energetics of these intermediate steps, particularly the binding energies of OH*, O*, and OOH* to the catalyst surface, play crucial roles in determining the overall reaction kinetics and efficiency. The ideal catalysts should optimally balance the binding strengths of these intermediates to minimize the overpotential required for each step.

Recent advancements in computational chemistry and *in situ* spectroscopic techniques have significantly enhanced our understanding of these reaction intermediates and their interactions with the catalyst surfaces. This improved insight has led to the development of more efficient OER catalysts, including transition metal oxides, perovskites, and nanostructured materials, each designed to optimize the energetics of the intermediate formation and transformation. Furthermore, the pH-dependent nature of OER has important implications for catalyst design and stability. Catalysts that perform well under alkaline conditions may degrade rapidly in acidic environments, necessitating careful consideration of the operational pH range for practical applications. Understanding and optimizing the OER mechanism across different pH ranges remains a central challenge in electrocatalytic research. Continued efforts in this area are crucial for advancing technologies such as water electrolyzers, metal-air batteries, and photoelectrochemical cells, all of which rely on efficient oxygen evolution for their operation.

The OER consists of four thermodynamically uphill steps, with the step having the highest energy barrier that determines the reaction potential. For an ideal catalyst, the thermochemical free energy required for each step is 1.23 eV [72,73]. However, studies on various metal oxides have shown that the actual free energy difference between the HOO* and HO* intermediates is approximately 3.2 ± 0.2 eV. This discrepancy highlights the challenges in achieving ideal catalysis.

To evaluate the catalytic activity of different catalysts, the difference in binding energy between O* (ΔG_{O^*}) and HO* (ΔG_{HO^*}) is utilized as a benchmark [74]. This parameter is crucial be-

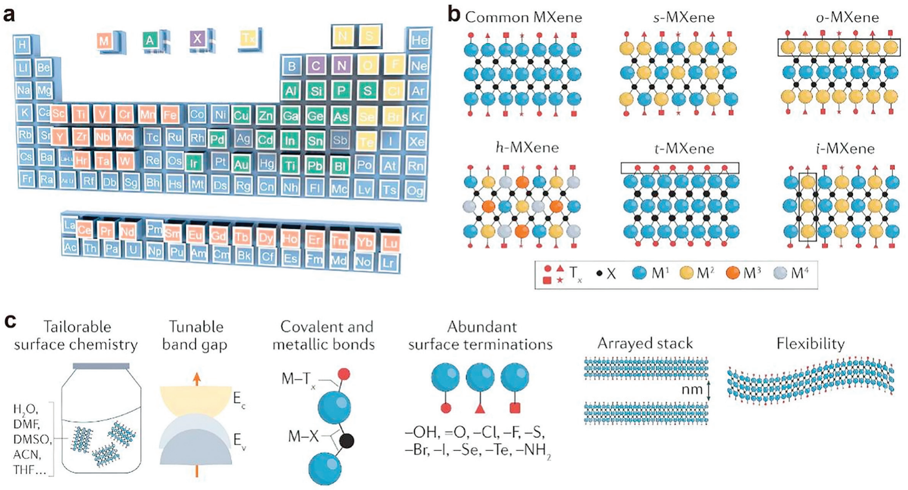

Fig. 1. (a) Periodic table of proper elements for the MAX phases. The elements of "M," "A," "X," and "T_x" are marked with orange, green, purple, and yellow colors, respectively. Reproduced with permission [75]. Copyright 2024, Springer Elsevier. (b) Six key MXene types. (c) Tailorable phase composition and surface chemistry result in diverse physicochemical properties. Reproduced with permission [76]. Copyright 2022, Springer Nature.

cause the bonding strength between the catalyst and oxygen species significantly influences catalytic activity. An optimal bonding strength is necessary, as excessively strong or weak bonds can lead to suboptimal reaction kinetics. Catalysts that exhibit balanced binding energies tend to perform better in OER catalysis. Using the $\Delta G_{O^*} - \Delta G_{HO^*}$ reference, researchers have constructed volcano curves for metal-oxide-based OER catalysts. This curve serves as a valuable tool for identifying trends in catalytic efficiency and for guiding the development of more effective OER catalysts. In the pursuit of cost-effective and abundant alternatives to precious metal-based catalysts, extensive research has been conducted on earth-abundant materials. While much of this research has focused on metal oxides and hydroxides, recent studies have explored transition metal chalcogenides and phosphides as promising OER catalysts. These materials often demonstrate superior OER activities compared to their corresponding oxide or hydroxide counterparts, partly because of their enhanced electrical conductivities. Ongoing exploration of such compounds continues to expand the portfolio of efficient and economical OER catalysts.

3. 2D MXenes

In 2011, Yury *et al.* [21] first discovered a novel two-dimensional material MXene, which is a layered structural material composed of metal carbides and/or nitrides with or without functional groups at the surface termini. Nearly 30 different compositions of MXenes have been synthesized, and theoretical predictions of the configurations of >100 MXenes have been made. The general chemical formula for MXenes is typically expressed as $M_{n+1}X_nT_x$, in which "M" denotes an early transition metal, "X" represents carbon or nitrogen, and "T_x" signifies a surface-terminating group such as -OH, -O, or -F [75,76], as displayed in Fig. 1. MXenes exhibit three-dimensional accordion-like particles arranged in a strict stack of two-dimensional lamellae. The unique localized three-dimensional individuals are arranged with a vacuum layer spacing of >1 nm, which can serve as active substance-bearing sites. MXenes can be prepared by selective etching of the element "A" in layered ternary carbides or nitrides (MAX phases) using a top-down approach. Because the bond energy of the M-A bond is weaker than that of the M-X bond, the addition of etching agents can be used to selectively remove the relatively weakly active A layer, leaving the chemically more stable $M_{n+1}X_nT_x$ layer. When the A elements are etched, the chemical activity and thermodynamics of the surface of the MXene layer tend to produce surface functional groups (T_x), which can thus be modulated according to various synthetic processes [77,78].

To date, nearly 30 different MXene compositions have been synthesized, with theoretical predictions suggesting the potential for over 100 configurations. This structural diversity, combined with their unique physical and chemical properties, positions MXenes as highly promising materials for a wide range of applications, particularly in the fields of energy storage, catalysis, and electronics. The ability to fine-tune surface terminations and interlayer spacing offers unprecedented opportunities for tailoring MXene properties to specific technological needs, driving continued research and innovation in this rapidly evolving field.

MXenes exhibit a diverse structural landscape categorizable into six major groups, with the first and most prevalent group consisting of common MXenes characterized by identical metal (M) elements and hybrid surface terminations. This group demonstrates remarkable versatility in the arrangement of transition metal sites, leading to three distinct types of isostructural MXenes: random solid solution MXenes (s-MXenes, *e.g.*, $Ti_{2-y}V_yCT_x$) [79] with stochastically distributed transition metals; out-of-plane ordered MXenes (o-MXenes, *e.g.*, $Mo_2Ti_2C_3T_x$) [80] featuring alternating layers of different transition metals; and in-plane ordered MXenes (i-MXenes, *e.g.*, $(Mo_{2/3}Y_{1/3})_2CT_x$) [81] with precisely arranged transition metals within the same atomic plane. This classification system not only highlights the structural complexity of MXenes but also underscores their potential for tailored properties through precise control of elemental composition and atomic arrangement, making them promising candidates for a wide range of applications from energy storage and catalysis to electronics [82]. The fifth major class is isostoichiometric MXenes capped with homogeneous halide or chalcogenide terminations (*t*-MXenes, *e.g.*, $Ti_3C_2Cl_2$). The last major class is high-entropy MXenes (*h*-MXenes, *e.g.*, $TiVNbMoC_3T_x$) with many M elements. The diversity of MXenes is greatly enhanced by the customizable combinations of many M elements [83,84]. This structural diversity is further amplified by the customizable combinations of various M elements, resulting in a wide array of physicochemical properties. Such structural complexity and compositional flexibility underscore MXenes' potential for tailored properties through precise control of elemental composition and atomic arrangement. This versatility positions

MXenes as promising candidates for a broad spectrum of applications, spanning from energy storage and catalysis to advanced electronics, driving continued research and innovation in materials science and technology.

MXene has a higher electrical conductivity among 2D materials. For example, the most studied $Ti_3C_2T_x$ has excellent electronic conductivity (almost 11,000 S/cm), while that of graphene oxide is only as high as 3000 S/cm. Owing to its abundance of surface functional groups, MXene is dispersible and can be dispersed at high concentrations in water and many common polar solvents, while maintaining a high level of conductivity (Fig. 1c). In addition, by modulating the types of transition metals and surface terminations, MXenes can display different electronic properties, ranging from metal-like states and semiconductors to insulators. The mechanical properties of electrocatalytic materials are important because of their complex reaction conditions. In terms of its mechanical properties, the precursor MAX phase of MXene is a very tough layered conductive ceramic, and after etching away the A layer, MXene still maintains its inherent tough ceramic properties with excellent rigidity and toughness.

MXene-based nanohybrids, as innovative materials for electrocatalytic water splitting, have garnered significant attention due to their remarkable properties that can be optimized for enhanced performance. One of the key advantages of MXenes is their tunable surface chemistry, which can be harnessed through surface functionalization. By selectively introducing functional groups (*e.g.*, -O, -OH, -F) onto the MXene surface, the wettability, charge distribution, and interaction with water molecules can be tailored. This modification can optimize the adsorption and desorption of reaction intermediates during water splitting, leading to improved reaction kinetics and higher catalytic activity. Combining MXenes with other functional nanomaterials, such as metals, metal oxides, or carbon-based materials, creates nanohybrids with enhanced properties. The choice of the secondary component and its interaction with MXenes play a crucial role in optimizing the electrocatalytic performance. For instance, incorporating transition metals or their oxides into MXene matrices can introduce additional active sites, improve charge transfer, and facilitate the desired reactions. Controlling the morphology of MXene-based nanohybrids, including their size, shape, and porosity, can significantly impact their electrocatalytic performance. Nanosized MXenes offer a larger surface area for charge transfer and reaction, while porous structures can facilitate the mass transport of reactants and products. By tuning these parameters, the accessibility of active sites and the overall catalytic efficiency can be optimized.

The interfaces between MXenes and other components in the nanohybrid are crucial for efficient charge transfer and catalytic activity. Interface engineering involves optimizing the interface structure, composition, and interactions to minimize energy barriers and promote charge flow. This can be achieved through precise control of the synthesis conditions, such as temperature, reaction time, and solvent choice, to ensure intimate mixing and strong interactions between the components. Introducing defects into the MXene lattice can create additional active sites and modify the electronic structure, enhancing the catalytic performance. Defects can be introduced through various methods, such as chemical etching, plasma treatment, or ion irradiation. The type, density, and distribution of defects can be tailored to optimize the catalytic activity and selectivity toward water splitting. In summary, optimizing MXene-based nanohybrids for electrocatalytic water splitting involves a multifaceted approach, including surface functionalization, compositional engineering, morphological control, interface engineering, defect engineering, and so on. By leveraging these strategies, researchers can design MXene-based nanohybrids with exceptional performance for sustainable hydrogen production.

4. MXene-based nanohybrids for HER

MXenes have attracted significant attention due to their unique physical and chemical properties, particularly in electrochemical reactions [85-91]. In the field of HER, the catalytic role of MXenes is particularly noteworthy. This article aims to provide a summary of the catalytic environment, conditions, types, and mechanisms of MXenes in alkaline/acidic HER.

Under acidic conditions, the HER over MXene-based catalysts is primarily triggered by proton discharge. The Volmer-Tafel mechanism is the most common, where Volmer involves the protonation of the active sites of the catalyst, followed by the Tafel reaction for hydrogen product ions. The acidic HER activity was much higher than that under alkaline conditions because of the easier dissociation of water molecules. The performance of MXene catalysts may also be affected by their various surface chemical properties. Different catalytic mechanisms can be observed, even for the same material. Under alkaline conditions, the HER of MXenes involves the Volmer-Heyrovsky or Volmer-Tafel steps. The Volmer reaction is the formation of adsorbed hydrogen atoms (H_{ads}) from water molecules on the catalyst active sites, primarily on the transition metal or surface functional groups of MXenes. The Heyrovsky and Tafel reactions involve the combination of Had with a water molecule or a combination of two H_{ads} on the catalyst surface to release hydrogen gas. The alkaline HER performance is influenced by several factors, including the water adsorption/dissociation ability, hydrogen binding energy, and adsorption strength of OH^- water solutions. Further enhancement of the catalytic activity can be achieved by adjusting the electronic structure and surface geometry of the catalysts.

MXene-derived catalysts, noted for their remarkable HER activities, often operate *via* distinct mechanisms. Specifically, those integrated with precious metals such as Ru_{SA}-N-$Ti_3C_2T_x$ and $PtO_aP_dO_b/Ti_3C_2T_x$ typically follow the Volmer-Tafel pathway. In contrast, highly active MXene-based catalysts, such as $Ni_{0.9}Co_{0.1}$@$Ti_{2.5}Nb_{0.5}C_2T_x$ and $Mo_2C/Ti_3C_2T_x$@NC, predominantly utilize the Volmer-Heyrovsky mechanism. Rarely, a hybrid approach is seen for catalysts such as BNNS/Ti_3C_2, which combines both mechanisms. It is worth mentioning that the energy favorability of these mechanisms can vary. For instance, some MXene catalysts may prefer the Volmer-Heyrovsky route because of the higher energy barrier of the Volmer-Tafel process. Conversely, if the Tafel step is energetically easier than the Heyrovsky step, the latter mechanism might be less favorable.

In essence, MXenes demonstrate considerable catalytic activity in both alkaline and acidic HER conditions. This proficiency is shaped by a multitude of considerations including the catalytic milieu, conditions, catalyst types, and underlying mechanisms. Delving deeper into these aspects and their interplay offers promise for refining the catalytic efficiency of MXenes, thus paving the way for advanced energy transformation and storage solutions.

4.1. Precious metal doped MXene for HER

Recent advances in water splitting catalysis have yielded several noteworthy studies [38,92], with Wu *et al.* [38] introducing a particularly innovative approach. They employed a rapid and continuous spray drying technique to fabricate crumpled $Ti_3C_2T_x$ MXene loaded with sub-nanometer platinum clusters (Pt/MXene) (Fig. 2). Scanning electron microscopy (SEM) reveals the three-dimensional crumpled structure of Pt/MXene (Fig. 2a), demonstrating that the incorporation of H_2PtCl_6 in the precursor solution does not compromise the product's unique morphology. Transmission electron microscopy (TEM) further corroborates this three-dimensional (3D) crumpled structure, providing additional insight into the catalyst's architecture. High-angle annular dark-field scanning transmission

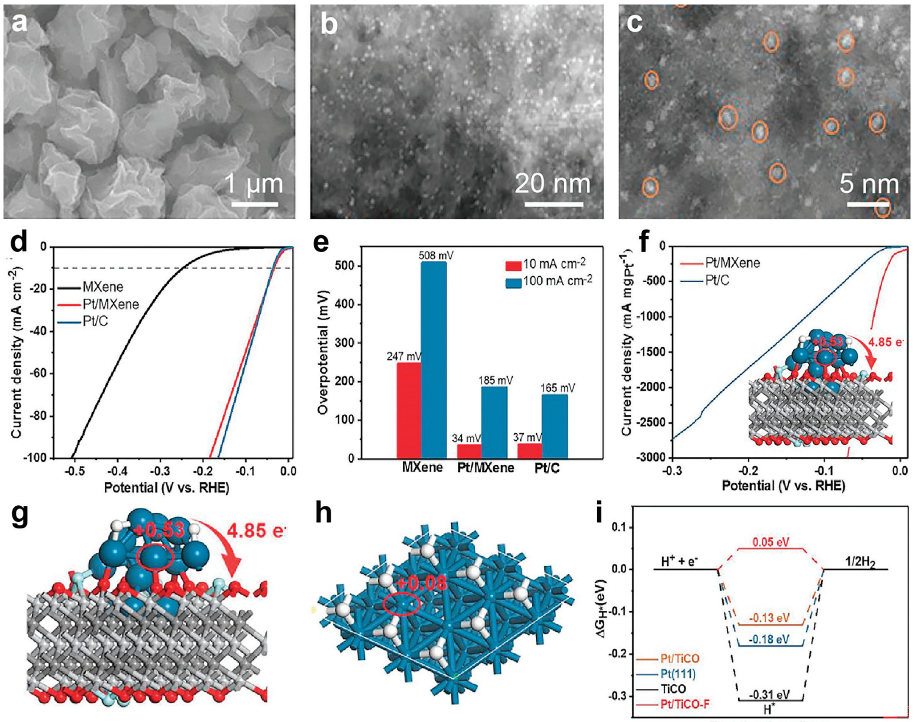

Fig. 2. (a) SEM images of Pt/MXene. (b, c) HAADF-STEM images of Pt/MXene. (d) Polarization curves. (e) Specific activity at the current density of 10 mA/cm^2 and 100 mA/cm^2, respectively. (f) Mass activity of Pt/MXene and Pt/C. Bader charge distribution of (g) Pt/TiCO-F and (h) Pt. Atoms in blue, white, red, cyan, gray, and dark gray represent Pt, H, O, F, Ti, and C, respectively. (i) The calculated free energy diagram for hydrogen evolution on Pt/TiCO, Pt(111), TiCO, and Pt/TiCO-F. Reproduced with permission [38]. Copyright 2022, Wiley.

electron microscopy (HAADF-STEM) offers a more detailed view of the catalyst's composition. This advanced imaging technique shows that sub-nanometer Pt clusters of uniform size are evenly distributed and firmly anchored on the MXene surface (Figs. 2b and c). Remarkably, the analysis also reveals the presence of isolated single-atom Pt species dispersed across the surface. This multifaceted characterization highlights the sophisticated structure of the Pt/MXene catalyst. The combination of the crumpled MXene substrate and the well-dispersed Pt clusters and atoms creates a high-surface-area catalyst with potentially enhanced catalytic activity. The uniform distribution of Pt species suggests efficient utilization of the precious metal, while the 3D structure may facilitate mass transport and increase the number of accessible active sites.

The HER performance of Pt/MXene was evaluated using representative three-electrode equipment in a 0.5 mol/L H_2SO_4 electrolyte with a virgin graphite rod as the counter electrode. Fig. 2d shows the HER polarization plots of S-$Ti_3C_2T_x$ MXene, Pt/C, and Pt/MXene. The S-$Ti_3C_2T_x$ MXene shows poor HER performance, and it requires an overpotential of 247 mV at the same current density of η_{10}. With the loading of Pt, Pt/MXene demonstrated a near-zero onset potential (η_{onset}) and the lowest overpotential of 34 mV to reach the specific current density (η_{10}). These results are comparable to those of state-of-the-art commercial Pt/C electrocatalysts (37 mV). At a higher current density of 100 mA/cm^2, Pt/MXene also exhibited a low overpotential of 185 mV (Fig. 2e). The current densities of Pt/MXene and Pt/C were normalized to the Pt loading to investigate the mass activity of the catalysts, which can more objectively reflect the catalytic activity.

Moreover, Pt/MXene exhibits much better HER performance in terms of mass activity compared to business-like 20 wt% Pt/C. Specifically, Pt/MXene demonstrated a mass activity of 1847 mA/mg$_{\text{Pt}}$ at an overpotential of 50 mV, which is seven times higher than that of Pt/C [38]. These results indicate that the Pt clusters anchored on 3D crumpled MXene are capable of delivering higher HER mass activity than industrialized Pt/C catalysts, and the 3D crumpled structure of MXene with maximized exposure of Pt is responsible for the superior mass activity. DFT calculations were employed to elucidate the intricate interactions between the platinum clusters and the MXene substrates (TiCO and TiCO-F). The study compared models of Pt/TiCO-F-H, Pt/TiCO-H, Pt(111)-H, and TiCO-H to gain comprehensive insights into their electronic and catalytic properties. Bader charge analysis revealed significant electron transfer from Pt clusters to the TiCO-F matrix, resulting in $a + 0.53$ positive charge per Pt site. This charge redistribution weakened the Pt-H bonding, a crucial factor in HER kinetics. The Gibbs free energy of hydrogen adsorption (ΔG_{H^*}) calculations further corroborated these findings. While TiCO exhibited strong hydrogen adsorption with ΔG_{H^*} of -0.31 eV, the Pt/TiCO-F system demonstrated a near-optimal ΔG_{H^*} of 0.05 eV, surpassing both Pt(111) (-0.18 eV) and Pt/TiCO (-0.13 eV). This optimal value for Pt/TiCO-F indicates a balance between hydrogen adsorption and desorption, crucial for efficient HER catalysis. The study concluded that the introduction of oxygen and fluorine termination groups on MXene effectively enhanced the interaction with Pt clusters, modifying their electronic states. This modification led to weakened hydrogen adsorption, facilitating easier hydrogen desorption and ultimately resulting in the superior HER catalytic activity observed in Pt/MXene systems. These findings provide valuable insights into the design principles for high-performance HER catalysts based on MXene-supported noble metal clusters.

In 2019, Jr-Hau He's group [93] reported a nitrogen and sulfur co-doping $Ti_3C_2T_x$ MXene coordinated Ru single-atom electrocatalyst synthesized by a lithium fluoride (LiF)/hydrochloric (HCl) acid leaching method followed by Freeze dry and annealing at Ar atmosphere. The as-prepared Ru_{SA}-N-S-$Ti_3C_2T_x$ catalyst displayed an excellent HER performance with a low overpotential of 76 mV to obtain the current density of 10 mA/cm^2. Also, the corresponding Tafel slope of the catalyst was confirmed to be 90 mV/dec, suggesting the Volmer-Heyrovsky mechanism and good reaction kinetics during the HER process. Moreover, the photoelectrochemical hydrogen production with a high photocurrent density of 37.6 mA/cm^2 was obtained by integrating the Ru_{SA}-N-S-$Ti_3C_2T_x$ catalyst on the n^+np^+-Si photocathode. The enhanced HER performances could be attributed to the Ru single-atom coordinated with N and S on $Ti_3C_2T_x$ MXene support.

In 2023, the HER electrocatalyst of Ru-RuO_2/MXene@CC prepared through etching of $Ti_3C_2T_x$ MXene and hydrothermal method was reported by Yan's group [52]. The Ru element content was adjusted to tune the hydrophilicity with the optimized water contact angle of 25.5. The Ru-RuO_2/MXene@CC with the Ru loading of 3 wt% showed good HER performances in alkaline media with a low overpotential of 43 mV to achieve the current density of 10 mA/cm^2 and a surpassingly low Tafel slope of 52.1 mV/dec, which transcended most reported MXene-based catalyst with a mass activity of 1751.11 mA/mg. Moreover, the Ru-RuO_2/MXene@CC catalyst displayed a good stability of 10 h at 10 mA/cm^2 to conduct HER. The excellent HER performances could be ascribed to the improved hydrophilicity, the enhanced diffusion capacitance, as well as the optimal ratio of Ru and RuO_2.

Most recently, a Pt NPs/d-$Mo_2Ti_2C_3T_x$ electrocatalyst to conduct HER was reported by S. Huang *et al.* [53]. The synthesis of Pt-based heterogeneous electrocatalysts concluded the preparation of $Mo_2Ti_2C_3T_x$ MXene, followed by the formation of Mo and oxygen vacancies on $Mo_2Ti_2C_3T_x$ MXene and the loading of ultrasmall Pt on the defect-enriched MXene. The defected enriched $Mo_2Ti_2C_3T_x$ supported Pt nanoparticles had an ultrasmall particle size of ~2.1 nm and high dispersity of Pt due to the anchoring by Mo vacancies and the large surface area of MXene. The as-synthesized Pt NPs/d-$Mo_2Ti_2C_3T_x$ electrocatalyst obtained an overpotential of 123 mV at the current density of 100 mA/cm^2 in 1.0 mol/L $HClO_4$ to conduct HER with the HER Faradaic efficiency of nearly 100% and a large turnover frequency of 8.49 H_2 s^{-1} at the overpotential of 50 mV, which was superior to that of the commercial Pt/C. Worth mentioning was that the mass activity of Pt on the Pt NPs/d-$Mo_2Ti_2C_3T_x$ electrocatalyst was confirmed to be 134 times higher compared to the commercial Pt/C. The electrons from Mo atoms could regulate the d-band electronic structure of Pt nanoparticles which strengthened the interaction with the absorbed H species and therefore boosted the HER performances.

4.2. Non-noble doped MXene for HER

While carbon-based precious metal electrocatalysts for HER demonstrate exceptional catalytic performance, their widespread application is hindered by high costs and scarcity of noble metals. This limitation has spurred intensive research into non-noble metal alternatives that could match or surpass the performance of their precious metal counterparts. A particularly promising approach involves the development of non-noble metal-doped nanocarbon materials as potential substitutes for precious metal-based HER electrocatalysts. In this pursuit, recent advancements in MXene research have garnered significant attention from the scientific community. MXenes, a class of two-dimensional transition metal carbides, nitrides, or carbonitrides, possess a unique combination of properties that make them exceptionally well-suited for electrocatalytic applications. Their distinctive layered structure, coupled with excellent chemical stability, superior electrical conductivity, and large active surface area, positions MXenes as highly promising candidates for next-generation HER electrocatalysts.

The growing interest in MXenes stems from their potential to address the key challenges faced by current HER catalysts. By offering a more abundant and cost-effective alternative to noble metals, while maintaining high catalytic activity, MXenes could pave the way for more sustainable and economically viable hydrogen production technologies. This development aligns with the broader goal of transitioning to clean energy sources and highlights the critical role of materials science in advancing renewable energy technologies. As research in this field progresses, the focus is on optimizing the composition, structure, and surface properties of MXenes to further enhance their HER performance. The versatility of MXenes, combined with their impressive intrinsic properties, opens up new avenues for designing efficient, durable, and scalable electrocatalysts. This ongoing work not only promises to revolutionize HER catalysis but also exemplifies the broader potential of novel materials in addressing global energy challenges.

A. Patra *et al.* [40] successfully fabricated a robust interface between orthorhombic $CoSe_2$ nanorods and two-dimensional $Ti_3C_2T_x$ MXene sheets, resulting in an amalgamated catalyst known as CSEMX (Figs. 3a-c). As shown in Fig. 3a, the texture of CSEMX where on the surface, and the surface the intrusion of CSE rods can be found seamlessly. The intercalation of $CoSe_2$ (labeled as CSE) rods into the sheets of MXene can be efficacious for the catalytic properties by the smooth charge transfer. HER performances of the catalysts are assessed in a three-electrode system in the 0.5 mol/L H_2SO_4 electrolyte. As displayed in Fig. 3b, the CSEMX nanohybirds exhibited exceptional catalytic activity, as evidenced by its low overpotential of 230 mV and a Tafel slope of 65 mV/dec for efficient HER (Fig. 3c). In comparison, the commercially purchased Pt/C electrode achieved the lowest overpotential of 35 mV, while CSE and MXene demonstrated higher overpotentials of 360 and 726 mV, respectively. Furthermore, the Tafel slopes for CSE and MXene were found to be 78 and 135 mV/dec, respectively, highlighting the superior kinetic metrics of the CSEMX catalyst (Fig. 3c). Additionally, the low R_{ct} value observed for CSEMX indicated rapid electrochemical kinetics and barrier-free charge transfer characteristics, surpassing those of the pristine CSE and MXene. These findings, along with the catalyst's maintained performance during a long-term stability test lasting over 12 h, underscored its durability and potential for practical HER applications. These findings demonstrate the synergistic effect achieved by combining $CoSe_2$ nanorods with MXene sheets in the CSEMX catalyst. The remarkable catalytic activity, favorable kinetics, and long-term stability of CSEMX position it as a promising candidate for next-generation HER catalysts, potentially advancing the field of sustainable hydrogen production.

Similarly, Hao *et al.* [54] reported on a highly active and cost-effective $Ti_3C_2T_x$-modified ZIF-8 ($Ti_3C_2T_x$@ZIF-8) catalyst that demonstrated remarkable electrochemical performance in an alkaline environment (Figs. 3d-f). As displayed in Fig. 3d, the $Ti_3C_2T_x$@ZIF-8 catalyst revealed a mixed morphology of $Ti_3C_2T_x$ (2D nanosheets) and ZIF-8 (highly textured surface with distinct crystal faces and a characteristic round ball-like shape [94,95]. The $Ti_3C_2T_x$@ZIF-8 has a combined morphological characteristic which further assures the successful combination of both elements in terms of surface features toward the desired electrochemical application. As a result, the $Ti_3C_2T_x$@ZIF-8 catalyst achieved an overpotential of 507 mV at 20 mA/cm^2 (Fig. 3e) and exhibited a Tafel slope of 77 mV/dec (Fig. 3f), which is significantly lower than the values observed for pristine $Ti_3C_2T_x$ (101 mV/dec) and ZIF-8 (143 mV/dec) in previous investigations. This comparison highlights the faster reaction rate of the $Ti_3C_2T_x$@ZIF-8 electrocatalyst compared to its components. To further evaluate the durability and stability of the synthesized material, a chronopotentiometry test was conducted at a current density of 20 mA/cm^2. Notably, the $Ti_3C_2T_x$-modified ZIF-8 catalyst also boasted an impressive electrochemically active surface area of 122.5 cm^2, contributing to its enhanced catalytic ac-

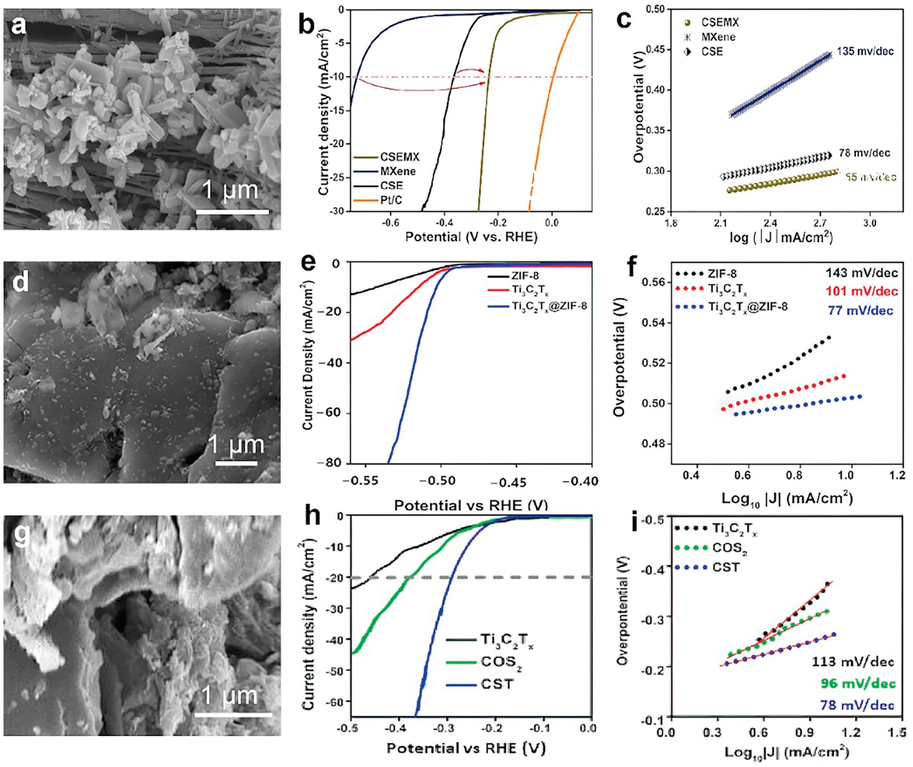

Fig. 3. (a) SEM image of CSEMX. (b) HER polarization curves of CSEMX, MXene, CSE, and Pt/C at the scan rate of 5 mV/s. (c) The corresponding Tafel slopes. Reproduced with permission [95]. Copyright 2022, Elsevier. (d) SEM image of $Ti_3C_2T_x$@ZIF-8. (e) HER polarization curves of $Ti_3C_2T_x$@ZIF-8, $Ti_3C_2T_x$, and ZIF-8. (f) The corresponding Tafel slopes. Reproduced with permission [41]. Copyright 2023, MDPI. (g) SEM image of CST. (h) HER polarization curves of CST, $Ti_3C_2T_x$, and COS_2. (i) The corresponding Tafel solpes. Reproduced with permission [95]. Copyright 2021, Elsevier.

tivity. The long-term stability test, lasting over 20 h, further underscored the catalyst's potential for energy conversion applications, as it maintained its performance without significant changes in overpotential.

Lv *et al.* [42] prepared a $Co_2P/N@Ti_3C_2T_x$@NF (CPN@TC) by controlling the grow of cobalt phosphates (Co_2P) on the surface of N-doped-$Ti_3C_2T_x$ MXene nanosheets-modified Ni foam (NF) by two-step electrodeposition. This electrocatalyst is notable for its multi-heterostructure interfaces and 3D porous structure, which contribute to its enhanced electrocatalytic activity. The CPN@TC electrocatalyst achieved an exceptionally low overpotential of 15 mV to reach a current density of 10 mA/cm^2, along with long-term stability and a small Tafel slope of 30 mV/dec in 1.0 mol/L KOH. Its performance rivals that of precious metal catalysts, thanks to its multi-heterointerfaces that facilitate the adsorption of H_2O and H*, as well as its excellent conductivity and well-designed structure that enable rapid ion and gas transport. Importantly, the synthetic strategy used for CPN@TC can be applied to the preparation of other transition-metal-based phosphides, offering a promising avenue for enhancing catalytic performance across a range of applications.

In addition, Hanan *et al.* [95] mixed CoS_2 and $Ti_3C_2T_x$ to form the CST nanohybrids by using a wet chemistry method with the addition of $Ti_3C_2T_x$ powder with various ratios. The CST exhibited excellent electrocatalytic properties in alkaline conditions. As shown in Fig. 3g, MXene flakes are embellished with tiny CoS_2 particles in the CST nanohyrids, improving surface characteristics and resulting in stronger electrochemical properties due to two distinguished elements [96]. The HER polarization curves of pristine $Ti_3C_2T_x$ and CoS_2 show their activity with higher overpotential values of 375 and 458 mV at a current density of 20 mA/cm^2. In contrast, the CST has shown better HER activity with a lower overpotential of 286 mV at 20 mA/cm^2 (Fig. 3h). The CST catalyst exhibited a Tafel slope value of 78 mV/dec, which favorably compares to the values of 96 and 113 mV/dec for CoS_2 and $Ti_3C_2T_x$, respectively. This lower Tafel slope indicates more efficient HER kinetics for the CST catalyst (Fig. 3i). Furthermore, it maintains a stable nature without any significant potential loss or fluctuation. This exceptional performance is complemented by a high electrochemical surface area (ECSA) of 495 cm^2 and a low charge transfer resistance (R_{ct}) of 115 Ω. These results confirm the CST catalyst's potential as a promising and durable electrocatalyst for HER, making it a viable candidate for future HER applications in alkaline media [43].

4.3. MXene-based nanohybrids for HER

MXenes have emerged as promising substrates for electrocatalytic HER applications, owing to their superior carrier mobility and larger surface area compared to conventional materials like graphene. To fully harness their potential, MXenes can be strategically hybridized with polymers, metal oxides, or metal sulfides. This hybridization serves a dual purpose: Preventing aggregation and mitigating mechanical stress. Moreover, MXenes offers the unique ability to fine-tune the electrophilicity of active sites, thereby optimizing the electrocatalytic performance of MXene-based nanohybrids. As a result of these advantages, recent studies have reported exceptional electrocatalytic activity of MXene-based nanohybrids in HER catalysis, underscoring their significance in advancing sustainable energy technology [97,98].

Li *et al.* [55] synthesized an efficient and stable MoS_2-Ti_3C_2 MXene electrocatalyst using a delicately designed one-step hydrothermal method, in which the few-layers thick, edge-oriented, high-percentage 1T'-phase (~85.0%) MoS_2 nanosheets are well grown

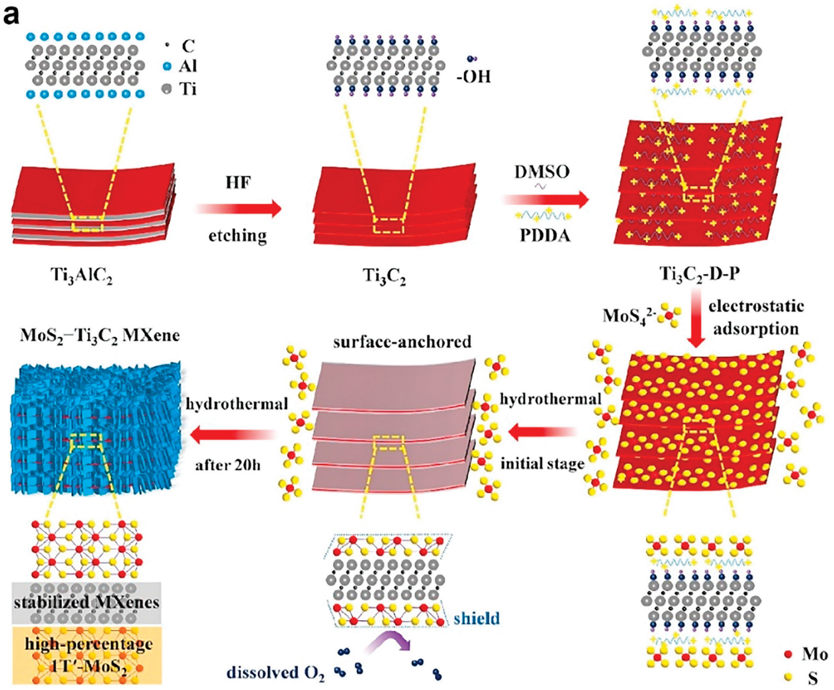

Fig. 4. Schematic illustration of synthetic route for MoS_2-Ti_3C_2 MXene hybrids. Reproduced with permission [55]. Copyright 2021, Elsevier.

on the cation-modified Ti_3C_2 MXene and stabilize Ti_3C_2 MXene against spontaneous oxidation caused by dissolved-oxygen. In detail, as shown in Fig. 4, the synthesis of the MoS_2/Ti_3C_2 nanohybrids involves a multi-step process that begins with the targeted etching of Al layers from Ti_3AlC_2 using HF acid to produce Ti_3C_2 MXene. This is followed by a pretreatment phase where Ti_3C_2 MXene is subjected to continuous stirring with PDDA cations and DMSO molecules. The positively charged PDDA cations adsorb onto the surface and intercalate between the Ti_3C_2 MXene sheets through electrostatic interactions, while DMSO molecules also penetrate the interlayer spaces. This pretreatment modifies the surface charge of Ti_3C_2 MXene, creating a positively charged Ti_3C_2-D-P complex that facilitates the subsequent adsorption and insertion of MoS_4^{2-} ions. These ionic precursors spontaneously and uniformly distributed across the surface and interlayer regions of the Ti_3C_2 MXene. During the initial stages of hydrothermal reaction, the pre-adsorbed MoS_4^{2-} ions form a protective MoS_2 shield on the surface, which plays a crucial role in preserving the structural integrity of Ti_3C_2 MXene by shielding it from oxygen. The hydrothermal process, conducted over 20 h, culminates in the uniform growth of few-layer thick, edge-oriented, 1T'-phase MoS_2 nanosheets on the stabilized Ti_3C_2 MXene substrate. This sophisticated synthesis strategy results in a well-integrated MoS_2/Ti_3C_2 nanohybrids material with enhanced structural stability and potential for improved electrocatalytic performance.

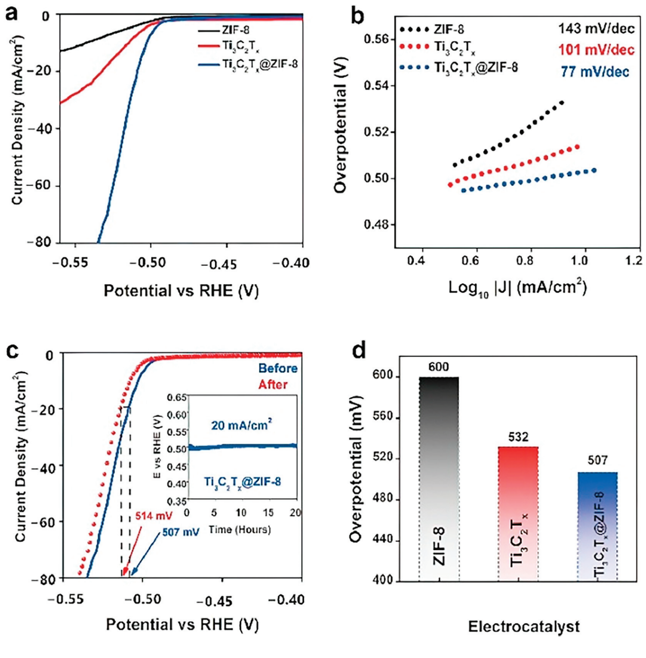

Fig. 5. (a) Polarization curves of Pt/C, Ti_3C_2 MXene, MoS_2-Ti_3C_2 MXene, MoS_2/oxidized Ti_3C_2, MoS_2, and bare CP at a sweep rate of 5 mV/s in 0.5 mol/L H_2SO_4. (b) Onset potential and overpotential at 10 mA/cm^2. (c) Chronoamperometry curve of MoS_2-Ti_3C_2 MXene for HER in 0.5 mol/L H_2SO_4. (d) Cycling stability of MoS_2-Ti_3C_2 MXene for HER in 0.5 mol/L H_2SO_4. Reproduced with permission [55]. Copyright 2020, Elsevier.

The structure and phase engineering of MoS_2 as well as the fully surface-shielding Ti_3C_2 MXene endow the as-synthesized MoS_2-Ti_3C_2 MXene electrocatalyst with a wealth of accessible active sites and high electrical conductivity for HER together with excellent structure stability in acidic media, with a remarkably low overpotential of just 98 mV to achieve a current density of 10 mA/cm^2, coupled with an impressively small Tafel slope of 45 mV/dec. Furthermore, the nanohybrids display minimal electrochemical resistance, indicating efficient charge transfer kinetics. These outstanding electrochemical properties collectively position the MoS_2-Ti_3C_2 MXene nanohybrids as a highly promising candidate for next-generation HER catalysts, potentially rivaling the performance of precious metal-based catalysts while offering the advantages of earth-abundant materials. The synergistic interaction between the edge-oriented MoS_2 nanosheets and the conductive Ti_3C_2 MXene substrate likely contributes to this enhanced catalytic activity, showcasing the effectiveness of the novel synthesis strategy in creating high-performance electrocatalysts for clean energy applications.

As illustrated in Fig. 5a, when juxtaposed with other candidate materials such as commercial Pt/C, pristine Ti_3C_2 MXene, oxidized

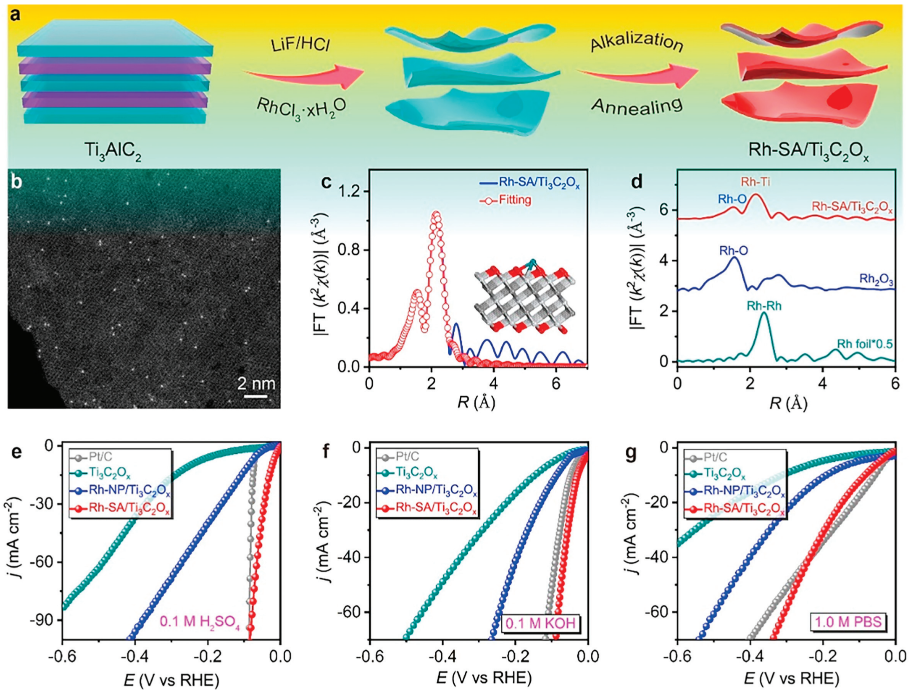

Fig. 6. (a) The scheme of the synthesis of $Rh-SA/Ti_3C_2O_x$. (b) Aberration-corrected HAADF-STEM image. (c, e) FT-EXAFS k^2-weighted $\chi(k)$ function spectra of $Rh-SA/Ti_3C_2O_x$ and the reference samples. (d) The corresponding FT-EXAFS fitting curves of $Rh-SA/Ti_3C_2O_x$. HER polarization curves in (e) 0.1 mol/L H_2SO_4, (f) 0.1 mol/L KOH, and (g) 1.0 mol/L PBS electrolyte, respectively. Reproduced with permission [61]. Copyright 2020, Royal Society of Chemistry.

Ti_3C_2, isolated MoS_2, and bare carbon paper (CP), the MoS_2-Ti_3C_2 MXene nanohybrids stands out with its diminished onset potential and overpotential. Notably, the nanohybrids catalyst attains an overpotential of a mere 98 mV at a current density of 10 mA/cm^2, as depicted in Fig. 5b. This performance surpasses that of most MoS_2-based catalysts reported in the literature, including those with metallic 1T or 1T' phases and 2H phases, as well as other conventional HER electrocatalysts. Moreover, the MoS_2-Ti_3C_2 MXene nanohybrids exhibit an impressively low Tafel slope of 45 mV/dec, a strong indicator of the catalyst's rapid electrochemical reaction kinetics. In terms of long-term stability, the MoS_2-Ti_3C_2 MXene nanohybrids have proven their mettle. Chronoamperometry tests, which were carried out over an extended period of 20 h, revealed that the catalyst retained 96.5% of its initial current (Fig. 5c). This retention rate is a testament to the catalyst's remarkable durability. Additionally, continuous CV scans served to validate the stability of the MoS_2-Ti_3C_2 MXene nanohybrids in a 0.5 mol/L H_2SO_4 solution, with no perceptible decline in performance (Fig. 5d). The findings collectively suggest that the MoS_2-Ti_3C_2 MXene nanohybrids catalyst is not only superior in terms of catalytic activity but also possesses commendable stability and durability, positioning it as a formidable contender in the field of electrocatalysis for energy conversion applications.

Peng *et al.* [61] have introduced a groundbreaking self-driven dual hydrogen production system that synergistically couples a Zn-H_2 battery with overall water/hydrazine splitting units. This innovative approach enables simultaneous and efficient hydrogen generation at the cathodes of both the Zn-H_2 battery and the overall hydrazine splitting (OHzS) units. The system's exceptional performance is attributed to the use of a novel bifunctional catalyst: single-atom rhodium immobilized on oxygen-functionalized $Ti_3C_2O_x$ MXene ($Rh-SA/Ti_3C_2O_x$, Figs. 6a-d). Remarkably, $Rh-SA/Ti_3C_2O_x$ demonstrates exceptional performance as a catalyst for HER, requiring mere overpotentials of 23 mV in 0.1 mol/L H_2SO_4, 85 mV in 1.0 mol/L PBS, and 29 mV in 0.1 mol/L KOH to achieve a substantial current density of −10 mA/cm^2 (Figs. 6e-g). These values are highly competitive, even rivaling those achieved by the benchmark Pt/C catalyst. Furthermore, $Rh-SA/Ti_3C_2O_x$ shines in alkaline hydrazine oxidation reaction (HzOR), delivering an impressive current density of 37.5 mA/cm^2 at a modest working potential of 0.1 V *vs.* RHE. Under ambient conditions, this system achieves a remarkable hydrogen generation rate of 45.77 mmol/h, significantly surpassing previously reported values for self-driven hydrogen production systems. This record-breaking performance stems from two key factors: The ingenious coupling of the Zn-H_2 battery with the overall hydrazine splitting system, and the outstanding electrochemical properties of the single-atomic Rh catalyst. The latter exhibits platinum-like catalytic activity towards both pH-universal HER and HzOR. In-depth experimental studies and DFT calculations reveal the mechanism behind the catalyst's exceptional performance. The atomically dispersed Ti–Rh–O_3 active sites significantly reduce the free energy changes associated with both hydrogen adsorption and the dehydrogenation of adsorbed $^*NHNH_2$ on $Rh-SA/Ti_3C_2O_x$. This energetic optimization renders both the HER and HzOR pathways highly favorable on the designed catalyst. This breakthrough not only underscores the critical importance of fine-tuning the local environment surrounding single-atom catalysts but also establishes a new paradigm for the rational design of high-performance HER catalysts. By meticulously engineering the interface between metal single atoms and support materials, researchers can now fully harness the potential of single-atom catalysts, pushing the boundaries of energy conversion and storage technologies. The implications of this research extend beyond immediate applications in hydrogen production. It opens new avenues for catalyst design, emphasizing the power of atomic-level engineering in creating highly efficient, multifunctional catalytic systems. As the field progresses, such innovations are likely to play a crucial role in addressing global energy challenges, paving the way for more sustainable and efficient energy solutions.

Furthermore, Peng *et al.* [62] expanded their pioneering work by developing a $Ti_3C_2T_x$ MXene-supported single Pt atom cat-

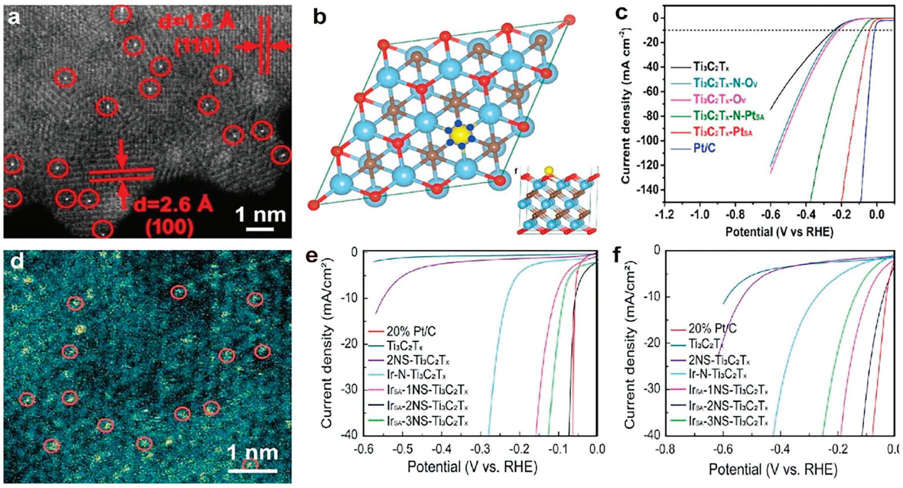

Fig. 7. (a-c) Aberration-corrected HAADF-STEM image, atomic structures, and HER curves of $Ti_3C_2T_x$-Pt_{SA}, Reproduced with permission [63]. Copyright 2022, American Chemical Society. (d) Aberration-corrected HAADF-STEM image of Ir_{SA}-2NS-$Ti_3C_2T_x$. HER curves in (e) acidic and (f) alkaline electrolytes, respectively, Reproduced with permission [64]. Copyright 2022, Royal Society of Chemistry.

alyst tailored specifically for HER. In this innovative design, Pt atoms are directly coordinated with O and Ti atoms, forming a unique catalyst denoted as Pt-SA/MXene. Leveraging the asymmetric coordination-induced local electric field polarization, Pt-SA/MXene significantly reduces the potential barrier for HER, thereby enhancing its activity in alkaline electrolytes. Notably, in 1.0 mol/L KOH, Pt-SA/MXene achieves a remarkable HER performance, requiring a mere 33 mV overpotential to attain a current density of 10 mA/cm^2, while maintaining this performance for over 27 h. Moreover, Pt-SA/MXene boasts a competitive mass activity of 23.5 A/mg$_{Pt}$ at an overpotential of 100 mV, surpassing commercial Pt/C catalysts by a factor of 29.4. This remarkable performance underscores the efficacy of the designed catalyst. Complementing these experimental findings, DFT calculations elucidate that the unique three O and one Ti atoms-coordinated configuration of each Pt site in Pt-SA/MXene optimize the adsorption of reactants and intermediates, aligning the HER pathway on the catalyst along an energetically favorable process. This comprehensive understanding not only deepens our knowledge of single-atom catalysts but also paves the way for the rational design of highly efficient HER electrocatalysts.

Gong *et al.* [63] successfully constructed a Pt single-atom catalyst anchored on the oxygen vacancies (O_V) of $Ti_3C_2T_x$ MXene ($Ti_3C_2T_x$-Pt_{SA}), employing an innovative rapid thermal shock methodology under a H_2 atmosphere (Figs. 7a-c). The $Ti_3C_2T_x$-Pt_{SA} exhibited remarkable performance in HER, surpassing the benchmark 20 wt% Pt/C catalyst in terms of both mass activity and turnover frequency (TOF). Through a meticulous blend of experimental observations and theoretical insights, it has been unveiled that the strategic positioning of Pt SAs on the O_V of $Ti_3C_2T_x$ MXene creates an exceptionally active site for HER catalysis. This unique configuration facilitates a swift and efficient hydrogen adsorption-desorption cycle, attributed to the minimal binding energy between hydrogen atoms and Pt SAs, along with a weakened hybridization strength compared to those observed with pristine $Ti_3C_2T_x$ MXene. This optimized coordination environment leads to a reduction in energy barriers, enabling faster reaction kinetics and enhanced catalytic efficiency.

Tan *et al.* [64] have developed a novel electrocatalyst consisting of Ir single atoms confined within a porous, heteroatom-doped $Ti_3C_2T_x$ MXene matrix, where nitrogen (N) and sulfur (S) serve as co-dopants (Figs. 7d-f). The researchers employed advanced characterization techniques, notably X-ray absorption spectroscopy (XAS), to elucidate the unique structural features of this catalyst. XAS revealed the *in situ* formation of a new bridging structure where Ir atoms are coordinated with both N and S atoms, facilitating the exceptional dispersion of Ir atoms throughout the porous N, S-doped $Ti_3C_2T_x$ MXene matrix. This precisely engineered atomic arrangement translates into remarkable catalytic performance, with the optimized Ir_{SA}-2NS-$Ti_3C_2T_x$ catalyst exhibiting outstanding HER activity in both acidic (0.5 mol/L H_2SO_4) and alkaline (1.0 mol/L KOH) electrolytes. The catalyst achieves impressively low overpotentials of 57.7 mV and 40.9 mV at a current density of 10 mA/cm^2 in acidic and alkaline media, respectively, positioning it among the most efficient HER catalysts reported to date. To gain deeper insights into the underlying mechanisms of this enhanced catalytic activity, the team conducted detailed DFT calculations. These theoretical investigations revealed a crucial electron transfer process from the Ir single atoms to the N, S co-doped $Ti_3C_2T_x$ support, leading to a significant charge redistribution in the interfacial region. This electronic modulation is postulated to be a key factor in the catalyst's exceptional HER performance. The study not only demonstrates a novel approach to single-atom catalyst design but also underscores the importance of supporting material engineering in maximizing catalytic efficiency. By synergistically combining the catalytic prowess of Ir single atoms with the tailored electronic properties of the heteroatom-doped MXene support, this research opens new avenues for the development of high-performance, atom-efficient electrocatalysts for clean energy applications.

5. MXene-based nanohybrids for OER

OER is the crucial electrochemical process occurring in water splitting technology, characterized by its intricate multistep electron and proton transfer processes. This complex reaction, involving the formation and transformation of oxygen-containing species, is profoundly influenced by catalyst properties and electrolyte conditions. The OER pathway diverges significantly across pH levels: in alkaline environments, it typically begins with water molecule adsorption on the catalyst surface, followed by proton-coupled electron transfers; whereas in acidic media, the initial step involves cleaving strong covalent bonds to form OH- intermediates. Optimizing OER efficiency demands meticulous catalyst design and synthesis. By fine-tuning materials and fabrication methods, researchers can tailor surface structures and electronic properties to enhance the adsorption and desorption of key intermediates. Concurrent optimization of electrolyte parameters (including pH, concentration, and temperature) further augments reaction kinetics and efficiency. Current research focuses on developing cost-effective, durable, and highly active OER catalysts. While precious metal oxides like RuO_2 and IrO_2 exhibit superior catalytic performance, their high costs and stability issues limit widespread application. This has spurred intense investigation into non-noble metal alternatives, such as transition metal oxides, hydroxides, sulfides, and phosphates. These materials offer diverse electronic structures and improved stability, holding promise for large-scale OER applications.

The quest for advanced OER catalysts is driving innovations at the intersection of materials science and electrochemistry. By elucidating reaction mechanisms and optimizing catalyst-intermediate interactions, researchers are not only advancing fundamental science but also paving the way for more efficient and sustainable water splitting technologies. This work has far-reaching implications for renewable energy systems, particularly in clean hydrogen production. As the field progresses, the development of next-generation OER catalysts is expected to play a pivotal role in realizing the full potential of water splitting as a key component of future clean energy infrastructures. These advancements could significantly contribute to addressing global energy challenges and accelerating the transition to a sustainable, hydrogen-based economy. The ongoing research in this domain exemplifies how targeted scientific inquiry can lead to transformative technologies with the potential to reshape our energy landscape and combat climate change.

5.1. Precious metal doped MXene-based nanohybrids for OER

Precious metal-doped MXene-based nanohybrids have emerged as a promising frontier in electrocatalysis, offering a unique combination of high catalytic activity, exceptional stability, and superior conductivity. Recent advancements in this field have centered on innovative strategies to further enhance their performance, including cation doping, oxygen vacancy engineering, and the introduction of tensile strain. These sophisticated modifications have led to remarkable improvements in OER activity, long-term stability, and overall durability, positioning precious metal-based MXenes as formidable alternatives to conventional electrocatalysts. The seamless integration of these advanced MXenes with nanostructured materials, such as FeOOH [99] and $RuSnO_x$ [62], has opened new avenues for designing highly efficient and robust electrocatalytic systems. This synergistic approach harnesses the intrinsic properties of MXenes while leveraging the complementary characteristics of other nanomaterials, resulting in hybrid catalysts with enhanced performance metrics.

As research in this domain continues to progress, precious-metal-based MXenes are poised to play a pivotal role in the development of next-generation sustainable energy conversion and storage technologies. Their unique properties and versatility make them ideal candidates for addressing the challenges associated with large-scale water splitting and fuel cell applications. The ongoing exploration of novel synthesis methods, precise compositional control, and innovative hybrid structures is expected to unlock even greater potential for these materials. The rapid advancements in precious metal-doped MXene electrocatalysts not only contribute to the fundamental understanding of catalytic processes but also have far-reaching implications for the broader field of renewable energy. As these materials continue to evolve, they hold the promise of enabling more efficient, cost-effective, and environmentally friendly energy systems, potentially accelerating the global transition towards a sustainable energy future.

Zhang *et al.* [44] developed a strategy that involved cation-doping and oxygen vacancy engineering to create Ru/Rh-doped FeOOH nanoarrays with abundant oxygen vacancies (Fig. 8a). These nanoarrays were grown *in situ* on $Ti_3C_2T_x$ MXene (Fig. 8b), resulting in a highly efficient OER electrocatalyst known as Ru/Rh-FeOOH@$Ti_3C_2T_x$. The optimized Rh/Ru-FeOOH@$Ti_3C_2T_x$ electrocatalysts exhibited exceptional OER activities and remarkable stabilities, lasting up to 100 h. Specifically, the 3%Rh-FeOOH@$Ti_3C_2T_x$ electrocatalyst required an overpotential of only 223 mV at 10 mA/cm^2 and 306 mV to reach 100 mA/cm^2 (Fig. 8c), surpassing the performance of commercial IrO_2 catalysts and many other reported oxyhydroxide-based electrocatalysts. The values of the calculated C_{dl} are14.49, 13.82, 3.74, and 1.63 mF/cm^2 for 3%Rh-FeOOH@$Ti_3C_2T_x$ MXene, 3%Ru-FeOOH@$Ti_3C_2T_x$ MXene, FeOOH, and FeOOH@$Ti_3C_2T_x$ MXene, respectively (Fig. 8d). So, the ECSA values of 3%Rh-FeOOH@ $Ti_3C_2T_x$ MXene, 3%Ru-FeOOH@$Ti_3C_2T_x$ MXene, FeOOH@$Ti_3C_2T_x$ MXene, and FeOOH are 362.25, 345.5, 93.5, and 40.75, respectively. The 3%Ru/Rh-FeOOH@ $Ti_3C_2T_x$ MXene possesses the biggest C_{dl}, unequivocally manifesting that Ru/Rh doping can expose more active sites, and the close heterogeneous interface between FeOOH and $Ti_3C_2T_x$ MXene is beneficial in increasing the catalytic active sites, thus facilitating the oxidation of water [100]. Through systematic theoretical calculations, kinetics, thermodynamics, and microstructural analysis, it was verified that the integration of Ru/Rh-cation doping and oxygen vacancies significantly enhanced the intrinsic conductivity and lattice defects of FeOOH. In turn, this exposed more active sites, reduced the adsorption/desorption energy barrier and activation energy, and improved the specific activity and catalytic kinetics of the electrocatalysts. Moreover, the *in situ* hybridization with MXene reinforced the structural stability of the electrocatalysts [44]. RuO_2 suffers from lattice oxygen participation and metal dissolution during the OER, compromising its durability. To overcome these limitations, Xu *et al.* [62] introduced tensile strain to the RuO_6 octahedrons within a binary Ru-Sn oxide matrix. This innovative approach weakened the covalency of the Ru-O bond, effectively preventing the involvement of lattice oxygen and the dissolution of Ru. As a result, the long-term stability of the electrocatalyst was significantly improved. Furthermore, the introduction of tensile strain optimized the adsorption energy of intermediates, leading to enhanced OER activity. In particular, the $RuSnO_x$ electrocatalyst exhibited remarkable OER performance in 0.1 mol/L $HClO_4$, requiring only a modest overpotential of 184 mV to achieve a current density of 10 mA/cm^2. Impressively, it maintained this current density for at least 150 h with minimal potential increase, demonstrating its exceptional durability [45].

Moreover, Gilbert Prince *et al.* [65] recently presented a solvothermal method for etching and exfoliating Ni-MAX to create Ni-MXene nanosheets, which serve as an efficient and non-noble electrocatalyst for OER. The synthesized Ni-MXene nanosheets, when applied as a catalyst over a nickel foam electrode (NiMX/NF), demonstrate an impressive overpotential of 245 mV at a current density of 100 mA/cm^2 (Fig. 8e). As illustrated in Fig. 8f, the overpotential of NiMX/NF at a current density of 100 mA/cm^2 is significantly lower compared to the contrast samples of commercial Pt-C/NF and NF, which exhibit overpotentials of 261 mV and 312 mV, respectively. The superior performance of NiMX can be ascribed to its 2D graphene-like morphology, wherein the layers are held together by weak van der Waals forces. This unique structure significantly enlarges the surface area, thereby exposing more active sites to the electrolyte and consequently enhancing the OER activity. The NiMX-loaded NF shows a much lesser Tafel slope value of 191 mV/dec as compared to Pt/C-loaded NF and bare NF. This indicates that the reaction kinetics is much faster in NiMX/NF as compared to Pt/C-loaded NF or bare NF (Fig. 8g). The excellent performance of the Ni-MXene catalyst can be attributed to two key

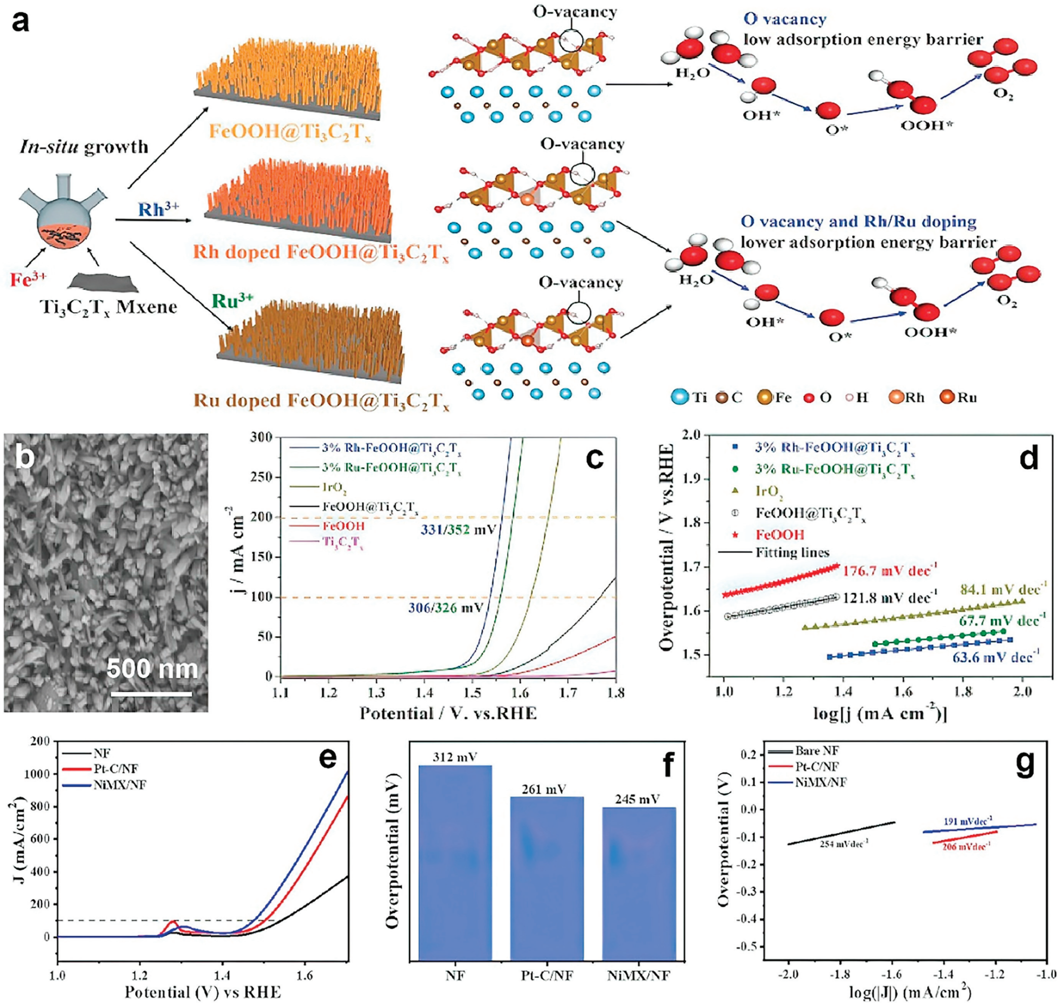

Fig. 8. (a) Schematic representation depicting the formation procedures of Ru/Rh-FeOOH@$Ti_3C_2T_x$ MXene and FeOOH@$Ti_3C_2T_x$ MXene, alongside their catalytic mechanism for the oxygen evolution reaction (OER). (b) SEM image of 3%Rh-FeOOH@$Ti_3C_2T_x$ MXene. (c) The OER polarization curves and (d) the corresponding Tafel slopes of various electrocatalysts in 1.0 mol/L KOH. Reproduced with permission [44]. Copyright 2022, Wiley. (e) OER LSV curves at the current density of 100 mA/cm^2. (f) Histogram indicating the difference in overpotentials, and (g) the corresponding Tafel slope of bare NF, Pt-C coated NF and NiMX loaded NF. Reproduced with permission [65]. Copyright 2022, Elsevier.

factors: the presence of the Ni$^{2+/3+}$ redox couple, which enhances electrocatalytic activity, and the carbon content in the nanosheets, which improves conductivity. Additionally, the catalyst electrode retains 83% of its initial current density after 14 h of continuous operation, highlighting its excellent stability [46].

5.2. Non-noble metal doped MXene for OER

In the quest for sustainable hydrogen production *via* electrocatalytic water splitting, the exploration of cost-effective, stable, and efficient non-noble metal catalysts has emerged as a pivotal avenue of research. Among these alternatives, non-noble metal-based catalysts supported on versatile 2D materials have garnered particular attention due to their unique electronic properties and tunable compositions. By harnessing the synergistic effects of various earth-abundant elements and the supporting matrix, these catalysts hold promise in overcoming the inherent challenges of high overpotential and sluggish kinetics associated with the OER. In this context, recent advancements in the design and synthesis of MXene-supported nanohybrids and nanohybrids have ushered in a new era of electrocatalysis, offering a compelling pathway toward the realization of large-scale and economically viable water splitting technologies.

Ye *et al.* [66] encapsulated ultrasmall NiFeP$_x$ nanoparticles in N-doped carbon and firmly anchored them on layered MXene nanosheets to form "continuous" single-crystal honeycomb-like MXene/NiFeP$_x$-NC nanohybrids by impregnation and phosphorization (Fig. 9a). This unique heterostructure consists of multi-layered $Ti_3C_2T_x$ MXene tightly anchoring ultrasmall NiFeP$_x$ nanoparticles encapsulated within the NC. The MXene and MXene/NiFe PB exhibit limited OER activity. In contrast, the MXene/NiFeP$_x$-NC heterostructure distinctly shines with its exceptional OER catalytic performance, attaining an overpotential of only 240 mV at a current density of 10 mA/cm^2. This superior performance surpasses that of NiFeP$_x$-NC (337 mV), MXene/$NiFe_2O_4$ (305 mV), and even commercial RuO_2 (290 mV) catalysts (Fig. 9b). The exceptional catalytic activity of the MXene/NiFeP$_x$-NC heterostructure can be attributed to its "continuous" single-crystal characteristics, abundant active sites derived from the ultrasmall NiFeP$_x$ NPs, and the stable honeycomb-like structure with an open framework. These findings are further supported by DFT calculations, which suggest that the unique MXene/NiFeP$_x$-NC heterostructure facilitates the sluggish OER, thereby ensuring outstanding durability and excellent activity with an ultralow overpotential [47].

Kang *et al.* [48] synthesized three bimetallic nanohybrids-Ni-Co (NCMX), Fe-Co (FCMX), and Fe-Ni (FNMX) onto MXene

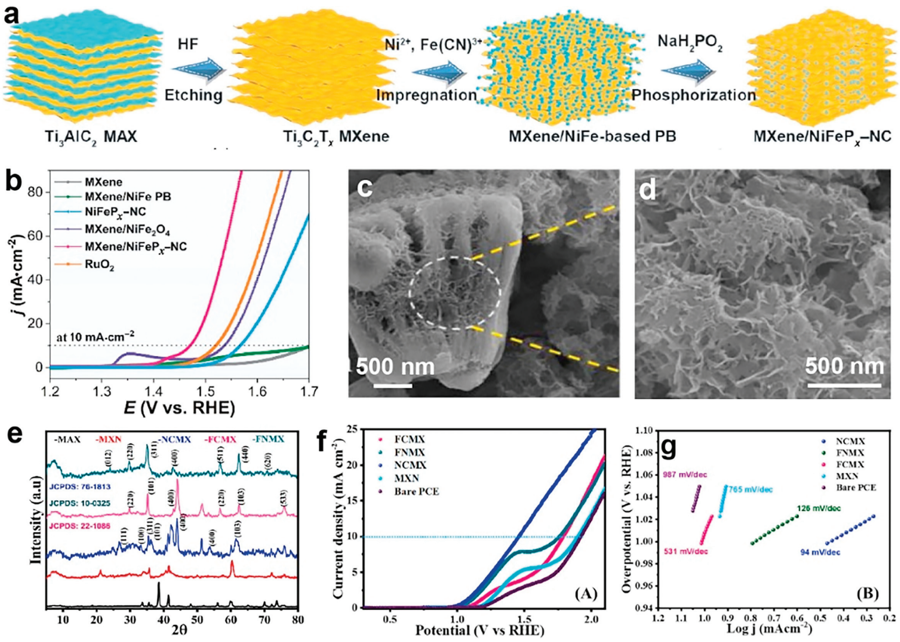

Fig. 9. (a) Schematic representation depicting the synthesis process of the MXene/NiFeP$_x$-NC electrocatalyst. (b) OER polarization curves of MXene, MXene/NiFe PB, NiFeP$_x$-NC, MXene/NiFe$_2$O$_4$, MXene/NiFeP$_x$-NC, and RuO$_2$ catalysts. Reproduced with permission [66]. Copyright 2022, the Author(s). (c, d) SEM images of NCMX nanohybrids. (e) XRD spectra. (f) OER LSV curves in 1.0 mol/L KOH at a scan rate of 5 mV/s. (g) The corresponding Tafel slopes. Reproduced with permission [48]. Copyright 2022, Elsevier.

for enhanced OER activity. The metal nanostructures were well-distributed and inter-connected *via* fusion on the MXene layers (Figs. 9c and d). To confirm the successful synthesis and phase transformation, X-ray diffraction (XRD) measurements were conducted. The absence of characteristic peaks at 2θ of 39°, corresponding to the (104) plane of the MAX phase (Ti$_3$AlC$_2$), implied the effective elimination of Al layers in forming the MXene (Fig. 9e). Moreover, the presence of Ni-Co complex peaks in NCMX confirmed the successful formation of NieCo nanohybrids on the MXene surface. To evaluate the catalytic performance, the synthesized nanohybrids were loaded onto a plastic chip electrode (PCE) and tested in a basic electrolyte (1.0 mol/L KOH). Among the catalysts, NCMX exhibited superior OER activity with a low overpotential of 220 mV (Fig. 9f). Additionally, Tafel slope analysis, derived from LSV curves, revealed that NCMX (94 mV/dec) had the lowest Tafel slope compared to FCMX (531 mV/dec), FNMX (126 mV/dec), and MXene (765 mV/dec) (Fig. 9g). This indicated a significantly faster reaction rate and improved OER kinetics for NCMX. The stability of the NCMX catalyst was further assessed using chronoamperometry and cyclic voltammetry techniques [48].

Li *et al.* [101] synthesized a carbon and nitrogen-doped porous Co$_2$P from ZIF-67, anchored on bimetallic MXene nanosheets to create MX@MOF-Co$_2$P. This innovative material was designed as an electrocatalyst for OER, a pivotal step in electrochemical water splitting. When the current density approached 100 mA/cm^2, the pristine Co MOF underwent rapid structural reorganization during the OER process, forming cobalt hydroxide and demonstrating improved activity with lower overpotential and Tafel slope. However, the MX@MOF-Co$_2$P catalyst surpassed this performance, exhibiting exceptional OER activity with low overpotentials of 246 mV at 10 mA/cm^2 and 407 mV at 200 mA/cm^2. Remarkably, its Tafel slope was only 28.18 mV/dec, significantly smaller than those of RuO$_2$@NF (86.87 mV/dec), Co MOF (54.65 mV/dec), Co$_2$P (45.96 mV/dec), and MOF-Co$_2$P (39.29 mV/dec), indicating much faster OER kinetics. This outstanding performance of MX@MOF-Co$_2$P was attributed to several key factors. Firstly, the porous structure of the original MOF provided a large number of open active sites, facilitating efficient catalytic reactions. Secondly, the modulation of the electronic structure of the active center by carbon and nitrogen doping further enhanced its catalytic activity. Lastly, the synergistic effect between cobalt phosphide and MXenes significantly improved electronic transfer, contributing to the overall superior performance of the catalyst. When compared to other reported similar catalysts, the synthesized MX@MOF-Co$_2$P stood out with its superior performance.

Du *et al.* [56] synthesized a novel CoNi-MOFNs@MXene nanohybrid *via* the *in-situ* growth of CoNi-MOFNs on Ti$_3$C$_2$T$_x$ MXene (Fig. 10a). Ensuring strong interfacial bonding and efficient charge transfer, which are imperative for enhanced OER electrocatalytic performance. The XRD, SEM, TEM, and EDS characterizations have confirmed the nanohybrids' intended morphology and uniform elemental distribution (Figs. 8b-e), providing a structural basis for its OER performance. Specificity, the peak presents a strong dependence on the ratio of Co/Ni as it shifts anodically and increases in intensity along with the increasing Ni content (Fig. 10f). The increased integrated area of these precatalytic oxidation peaks suggests an increase in the redox-active atoms. On the other hand, the shift of this redox peak can be further explained by the partial electron transfer from Ni^{2+} ion to Co^{2+} ion through the bridged oxygen atom in CoNi-MOFNs [102]. With the increase of Ni content and electron donation, the outflow of electrons from the Co^{2+} ion was inhibited. Upon consideration of the relationship between the variable numbers of redox-active atoms, shifting of precatalytic oxidation peaks, and the varying Co/Ni ratio, it is unveiled that in CoNi-MOFNs the redox behavior might be affected by a combination of multi-factors.

As displayed in Fig. 10g, the CoNi$_{40}$-MOFNs show the lowest overpotential of 346 mV to reach a current density of 10 mA/cm^2 than that of Co-MOFNs (443 mV), CoNi$_{10}$-MOFNs (377 mV), CoNi$_{20}$-MOFNs (369 mV), CoNi$_{30}$-MOFNs (367 mV, 66.8 mV/dec^2), and CoNi$_{50}$-MOFNs (359 mV), implying the improved OER activity which might be resulted from the electronic coupling between Ni and Co [103]. The Tafel slope analysis presented in Fig. 10h provides crucial insights into the electrocatalytic kinetics of various catalysts. It reveals a striking contrast between the monometallic and bimetallic catalysts. Co-MOFNs and Ni-MOFNs exhibit

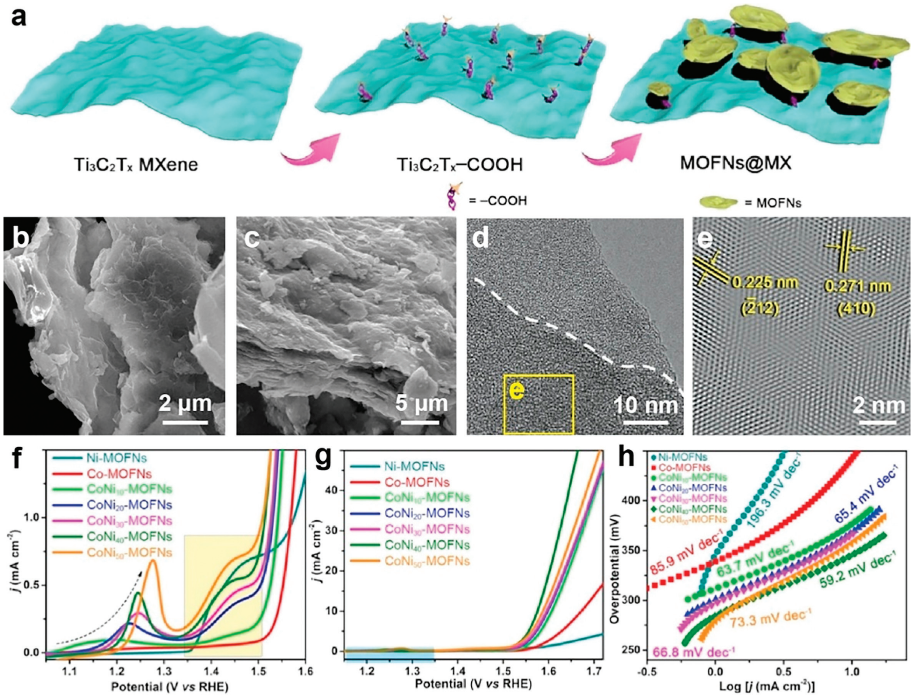

Fig. 10. (a) Scheme illustration of the preparation of the CoNi-MOFNs@MX nanohybrids. (b) SEM image $Ti_3C_2T_x$-COOH MXene nanosheets. (c) SEM and (d) TEM images of CoNi20-MOFNs@MX nanohybrid. (e) The inverse FFT image of the region which labeled in (d). (f, g) OER polarization curves. (h) The corresponding Tafel plots. Reproduced with permission [56]. Copyright 2021, Wiley.

relatively large Tafel slopes of 86.5 and 196.3 mV/dec, respectively, indicating slower reaction kinetics. In contrast, the CoNi-MOFNs compounds demonstrate significantly reduced Tafel slopes (59.2 mV/dec^2), suggesting a marked enhancement in electrocatalytic performance. In addition, the stability test results have demonstrated that the CoNi-MOFNs@MX maintains stability for over 40 h, a prerequisite for long-term applications. XPS analysis post-OER testing showed stable valence states of Co and Ni in $CoNi_{20}$−MOFNs@MX, indicating the material's stability and resistance to activity decay. The results demonstrated that the CoNi-MOFNs@MX nanohybrid has a high OER activity, rapid kinetics, and excellent stability, positioning it as a promising material in the field of electrocatalysis.

Zhao *et al.* [57] engineered a superior OER electrocatalyst by integrating dual Co/Ni atomic sites onto a $Ti_3C_2T_x$ MXene scaffold (CoNi-$Ti_3C_2T_x$). As shown in Figs. 11a-c, the bright well-dispersed spots in the aberration-corrected HAADF-STEM images prove the successful synthesis of atomic CoNi-$Ti_3C_2T_x$, $Ti_3C_2T_x$, and Co-$Ti_3C_2T_x$ electrocatalysts. This synthesis employed an avant-garde surface modification strategy utilizing L-tryptophan pre-adsorption, which engendered robust metal-support interactions and a substantial mass loading of 5.6 wt%, significantly augmenting the catalyst's intrinsic activity. For the OER performance texts, the CoNi-$Ti_3C_2T_x$ catalyst illustrated exceptional efficacy, necessitating an overpotential of merely 241 mV at 10 mA/cm^2, as delineated by LSV curves (Fig. 11d), which surpasses the performance of Ni-$Ti_3C_2T_x$ (298 mV), commercial RuO_2 (332 mV), and Co-$Ti_3C_2T_x$ (375 mV). The CoNi-$Ti_3C_2T_x$'s Tafel slope of 79.8 mV/dec (Fig. 11e) is indicative of its swift electrochemical kinetics. Electrochemical impedance spectra (EIS) data (Fig. 11f) corroborate these findings, with CoNi-$Ti_3C_2T_x$ demonstrating the lowest charge transfer resistance ($R_{ct} = 14.61\ \Omega$), underscoring its efficient charge transfer kinetics in the OER process.

In general, the optimized electrocatalytic performances of the electrocatalysts are highly related to their electronic structure, so the DFT was further performed. The charge density difference plots presented in Figs. 11g-i reveals that the Co and Ni centers in CoNi-$Ti_3C_2T_x$ exhibit decreased electron density, indicating a transfer of electrons from the Co/Ni atoms to the $Ti_3C_2T_x$ substrate. To quantitatively assess the electron variation within these nanohybrids, we conducted further calculations of the Bader charges for the three electrocatalysts. Compared to the single-atom catalysts (Co-$Ti_3C_2T_x$ and Ni-$Ti_3C_2T_x$), a greater number of electrons are donated from Co (0.41 |e|) and Ni (0.08 |e|) to the CoNi-$Ti_3C_2T_x$ substrate. This suggests that the synergistic interaction between Co and Ni atoms results in an enhanced degree of electron transfer. Overall, DFT calculations demonstrate that Ni and Co in CoNi-$Ti_3C_2T_x$ can collaboratively enhance electron modulation between the active sites (Co and Ni) and substrates, leading to lower energy barriers for the OER process [104,105].

Furthermore, the exploration of MXene-anchored single-atom catalysts for OER has garnered significant attention, primarily driven by first-principles investigations. For instance, Fan *et al.* [106] conducted a comprehensive investigation on a series of transition-metal atoms X (Ti, V, Cr, Mn, Fe, Co, Ni, Cu, Zn) supported by MXenes M_2NO_2 (M = Ti, V, Cr) as potential single atom catalysts for OER. Notably, among these single atom sites, Cu anchored on Ti_2NO_2 exhibited promising characteristics as an OER electrocatalyst, with an overpotential of only 0.24 V for the four OER reaction steps at Cu-Ti_2NO_2. To further understand the properties of this catalyst, the bonding strength between the Cu atom and supporting Ti_2NO_2 was examined, and ab initio molecular dynamics simulations (AIMD) were performed to assess the stability of Cu on Ti_2NO_2. Moreover, considering the significance of OER in metal-air batteries, where the active substance on the cathode is oxygen from the air, the adsorption of small molecules such as CO, NO, NO_2, SO_2, H_2O, and O_2 was calculated. In another study, Chen *et al.* [107] employed high throughput screening and identified MXenes as promising supports for single atoms to enhance OER efficiency. The stability of various MXenes was assessed based on specific formation energies, leading to the identification of seven potential MXene candidates including $Ti_3C_2(OH)_x$, $V_3C_2(OH)_x$, $Zr_3C_2(OH)_x$,

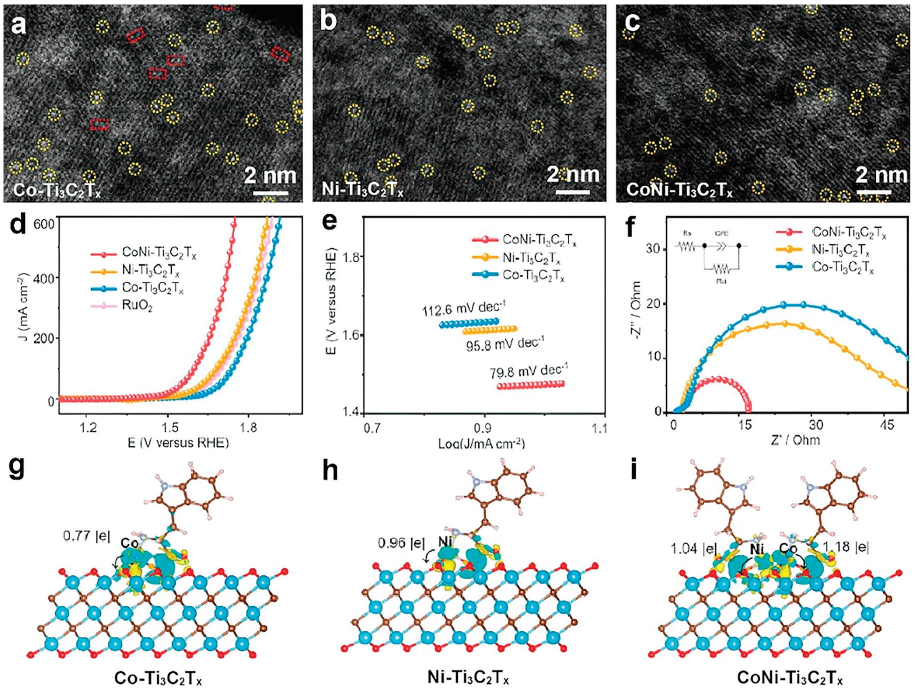

Fig. 11. (a-c) HAADF-STEM images of various electrocatalysts. (d, e) OER LSV curves at the scan rate of 5 mV/s and the corresponding Tafel slopes. (f) EIS Nyquist plots with the corresponding equivalent circuit shown in the inset. (g-i) Calculated total DOS and PDOS of the Ni d-band, Co d-band, and O p-band for these electrocatalysts. The d-band center is marked by red arrows for each case. The charge density difference and the calculated Bader charges of active sites for the electrocatalysts. The yellow and cyan colors indicate charge accumulation and depletion, respectively. Reproduced with permission [57]. Copyright 2024, Elsevier.

$Nb_3C_2(OH)_x$, $Hf_3C_2(OH)_x$, $Ta_3C_2(OH)_x$, and $W_3C_2(OH)_x$ as promising supports for single atoms. Subsequently, transition metal elements were evaluated for their suitability as single-atom elements. Metals such as Zn, Pd, Ag, Cd, Au, and Hg were excluded due to their high cohesive energies, indicating their exceptional stability. $Hf_3C_2(OH)_x$ with a Pd single atom delivers a theoretical overpotential of 81 mV. Both moderate electron-deficient state and high covalency of metal-carbon bonds were critical features for the high OER reactivity. Theoretical overpotentials for these MXene-based single-atom catalysts were determined through Gibbs free energy calculations. Further analysis of the structure-activity relationship was conducted using machine learning techniques, revealing that a moderately electron-deficient single-atom center and a highly covalent M-C bond are critical factors for optimal OER activity. This insight is expected to guide the rational design of efficient OER catalysts.

6. MXenes-based nanohybrids for overall water splitting

Electrocatalytic water splitting represents a cornerstone of renewable energy technologies, offering a clean and sustainable method to produce hydrogen fuel and oxygen through the fundamental processes of HER and OER. Ideally, these reactions necessitate a voltage difference of only 1.23 V. However, practical implementation often encounters an increased potential requirement, referred to as overpotential. This undesirable phenomenon significantly elevates the energy input necessary for water decomposition, thereby diminishing the process's overall efficiency. To surmount this critical challenge, researchers have explored the utilization of electrocatalysts capable of accelerating the kinetics of both HER and OER. These specialized materials function by reducing the activation energy barrier. They achieve this by adsorbing reactants, facilitating their conversion into products, and enhancing charge transfer kinetics. Among the diverse array of materials investigated for this purpose, a group of two-dimensional transition metal carbides, nitrides, and carbonitrides, collectively known as MXenes, have recently garnered substantial attention.

MXenes stand out due to their exceptional electronic properties, high conductivity, and tunable surface chemistry, which render them well-suited for dual-function HER/OER catalysis. Notably, the ability of MXenes to perform effectively in both reactions suggests the potential to employ them in direct seawater splitting. This capability would be transformative, as it could simplify the design of electrolysis cells and amplify the total efficiency of the water splitting procedure. Such advancements hold the promise of making electrocatalytic water splitting more cost-effective and sustainable, potentially fostering broader adoption of this renewable technology on a global scale. The ongoing research and development in this area aim to optimize the performance of MXenes, making them a key component in the future of renewable energy technology.

Chaudhary *et al.* [49] successfully fabricated bimetallic $NiCo_2Se_4$ (NCSe), MXene, and reduced graphene oxide (rGO) into a 3D hierarchical aerogel structure as NCSe@MGA by hydrothermal and wet-chemical methods. As shown in Figs. 10a-d, the NCSe precursor comprised of predominant urchin-like morphology constructed by densely aligned nanoneedles (Fig. 12a). After selenization, the urchin-like structure of the NCSe precursor evolved into a microsphere with a relaxed surface, the surface of which was formed by the aggregation of nanoparticles (Fig. 12b). The pore structures of NCSe@GA were characterized by irregular connections and crimpled cell walls (Fig. 12c). In contrast, the pores in NCSe@MGA exhibited a more regular arrangement with straighter cell walls (Fig. 12d). This distinction can be attributed to the stiffer nature of the MXene sheets, which serve as a scaffold and help to prevent the wrinkling of rGO sheets to a certain extent during their integration into the 3D network. The well-established network not only provides mechanical strength to NCSe@MGA but also protects it from deformation during processing. To further enhance the understanding of this concept, it is worth mentioning that the incorporation

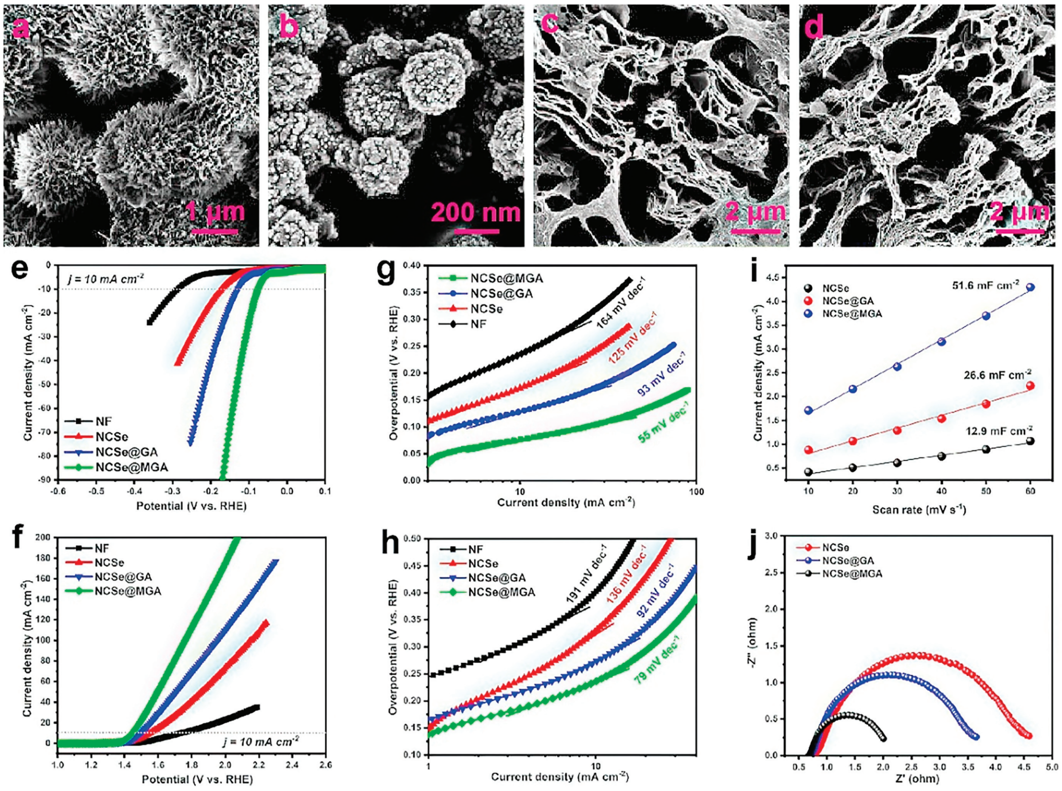

Fig. 12. SEM images of (a) NCSe precursor, (b) NCSe microspheres, (c) NCSe@GA, and (d) NCSe@MGA. (e) HER and (f) OER polarization curves and (g, h) the corresponding Tafel curves in 1.0 mol/L KOH electrolyte. (i) The C_{dl}. (j) EIS spectrum. Reproduced with permission [49]. Copyright 2022, Elsevier.

of MXene sheets into the rGO matrix results in a synergistic effect, where the unique properties of both materials are combined to create nanohybrids with improved characteristics. The stiffness of the MXene sheets helps to maintain the structural integrity of the rGO layers, preventing them from collapsing or folding in on themselves. This not only ensures a more uniform pore size distribution but also contributes to the overall mechanical stability of the NCSe@MGA nanohybrids.

These innovative nanohybrids not only accommodated strain during electrochemical tests but also prevented the pulverization of NCSe, thanks to the flexible skeleton of the Ti_3C_2 MXene@Graphene nanohybrids aerogel. In 1.0 mol/L KOH solution with a typical three-cell configuration, the polarization curves revealed that NCSe@MGA had an earlier onset of current for both HER and OER compared to Ni Foam, NCSe, and NCSe@GA. Specifically, NCSe@MGA achieved a current density of 10 mA/cm^2 at low overpotentials of 78 mV for HER (Fig. 12e) and 201 mV for OER (Fig. 12f), with Tafel slopes as low as 55 mV/dec (Fig. 12g) and 79 mV/dec (Fig. 12h), respectively. These results indicated fast kinetics and highlighted the exceptional performance of NCSe@MGA nanohybrids in electrocatalytic water splitting. Importantly, the enhanced electrochemical activity of NCSe@MGA could be attributed to the synergistic effects arising from the intimate contact between NCSe, MXene, and Graphene. Furthermore, the stability of NCSe@MGA was confirmed by the absence of significant decay in current density during a 10 h electrolysis test for both HER and OER. Overall, these findings highlighted the potential of NCSe@MGA as a highly efficient and stable electrocatalyst for water splitting applications. From the slope of plots (scan rate *vs.* current density) and EIS spectrum, it can be found that the NCSe@MGA has the largest value of C_{dl} (51.6 mV/cm^2, Fig. 12i) and the smallest value of R_{ct} (2.04 Ω, Fig. 12j), demonstrating its enriched active sites and better adsorption of H_2O molecules for HER.

Li *et al.* [50] developed an alloy-phase bimetallic sulfide anchored on the conductive substrate MXene supported on nickel foam (Co_8FeS_8 MXene/NF) by a one-step solvothermal method and a self-template sacrificial vulcanization process. The efficient nanohybrids electrocatalyst of Co_8FeS_8 MXene/NF with multimetal active sites exhibits extraordinary electrocatalytic performance with remarkably low overpotentials of 171 mV (OER) and 108 mV (HER) at 10 mA/cm^2, respectively. Notably, when used in 1.0 mol/L KOH electrolytic cell, Co_8FeS_8 MXene/NF also accelerates overall water splitting at an ultra-low cell voltage of only 1.51 V at 10 mA/cm^2, far exceeding that of standard Pt-C/NF//RuO_2/NF electrodes (1.59 V). DFT and related material characterization demonstrate that electron rearrangement at the atomic/orbital level and hierarchical electronic coupling between Schottky heterostructures of MXene boosts charge transfer efficiency, the asymmetric 3d electronic structure of the Co-Fe atoms optimizes the d-band center value of the Co_8FeS_8 MXene/NF [108,109]. This efficient strategy enables unprecedented improvements in the intrinsic properties of hybrid materials. When employed in a 1.0 mol/L KOH electrolytic cell for overall water splitting, the Co_8FeS_8 MXene/NF catalyst exhibits impressive performance. It requires an ultra-low cell voltage of only 1.51 V at 10 mA/cm^2, surpassing the performance of standard Pt-C/NF and RuO_2/NF electrodes, which demand a higher voltage of 1.59 V.

Similarly, Yu *et al.* [51] have developed an advanced electrocatalyst for water splitting by integrating ruthenium-cobalt bimetallic nanoalloys with exfoliated $Ti_3C_2T_x$ MXene to create the RuCo-$Ti_3C_2T_x$ nanohybrids, utilizing an ice-templated and thermal activation process for a strong coupling between the RuCo nanoalloys and the highly conductive MXene. The RuCo-$Ti_3C_2T_x$ electrocatalyst demonstrates exceptional performance for both the HER and OER. In acidic and alkaline media, it exhibits low overpotentials and Tafel slopes for HER, indicating fast kinetics. Additionally, it

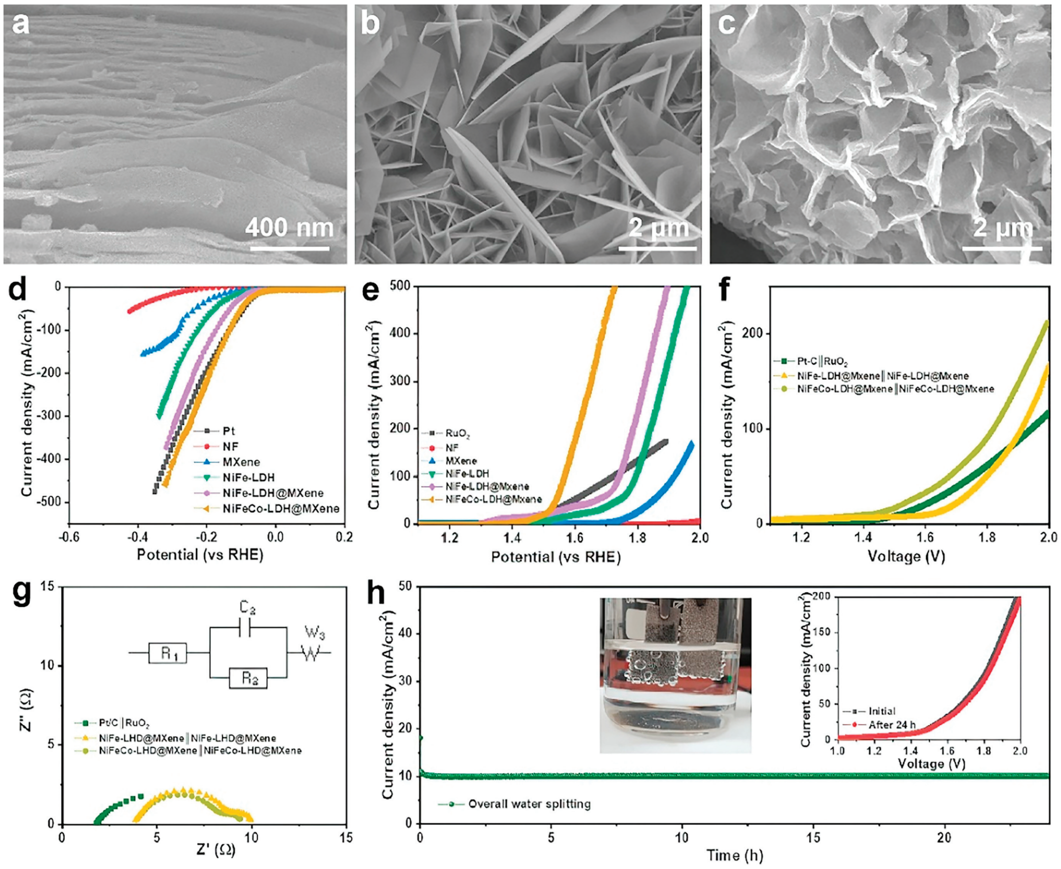

Fig. 13. (a) SEM image of the MXene. (b) SEM of the NiFe-LDH@MXene nanohybrids. (c) SEM image of NiFeCo-LDH@MXene nanohybrids. (d) HER and (e) OER LSV curves of bare NF, Pt/C, MXene, NiFe-LDH, NiFe-LDH@MXene, and NiFeCo-LDH@MXene at a scan speed of 10 mV/s. (f) Overall water splitting polarization profiles of the catalysts. (g) EIS profiles. (h) The variations in the time-dependent current density of the NiFeCo–LDH@MXene||NiFe–CoLDH@MXene device at a constant applied voltage for continuous water splitting operation over 24 h. Reproduced with permission [59]. Copyright 2022, Elsevier.

performs well for OER in alkaline electrolytes. When tested in a two-electrode electrolyzer configuration, the RuCo-$Ti_3C_2T_x$||RuCo-$Ti_3C_2T_x$ system requires a lower potential (1.56 V) than the benchmark Pt/C||RuO_2 electrolyzer at a current density of 10 mA/cm^2, highlighting its promise for practical water splitting applications.

Li *et al.* [54] introduced a novel and efficient bifunctional electrocatalyst for water splitting: The multiphasic 1T/2H $MoSe_2$ on MXene nanosheets heterostructure (1T/2H $MoSe_2$/MXene) (Figs. 10c and d). This innovative catalyst leverages the complementary strengths of 1T/2H $MoSe_2$ and MXene. In terms of HER performance, the 1T/2H $MoSe_2$/MXene electrode exhibits an overpotential of 95 mV at a current density of 10 mA/cm, which is significantly lower than that of 2H $MoSe_2$/MXene (123 mV), 1T/2H $MoSe_2$ (145 mV) and MXene (194 mV) alone. Similarly, for OER, the same catalyst achieves an overpotential of 340 mV at a current density of 10 mA/cm^2, which outperforms 2H $MoSe_2$/MXene (380 mV), 1T/2H $MoSe_2$ (397 mV), MXene (400 mV), is even comparable to commercial RuO_2 (320 mV) (Figs. 10e and f). This exceptional performance is further evident in the Tafel slopes observed for different samples. The Tafel slope of 1T/2H $MoSe_2$/MXene is notably lower (91 mV/dec for HER and 90 mV/dec for OER) than those of other electrodes, indicating more efficient electrocatalytic kinetics.

In the study conducted by Sajjad Hussain and colleagues, a honeycomb-like porous nanohybrid catalyst, NiFeCo-LDH@MXene, was innovatively engineered for efficient bifunctional overall water splitting [59]. The synthesis was achieved on a nickel foam platform through a simple hydrothermal process, showcasing remarkable electrocatalytic performance and stability in alkaline media. SEM images (Fig. 13a) exposed the layered sheet configuration of MXene, which was derived from the MAX phase Ti_3AlC_2 through an HF etching methodology. The SEM visualizations confirmed that the surface nanostructure was predominantly composed of dispersed sheets, which were identified as polycrystalline by FFT patterns aligning with XRD outcomes. An exhaustive investigation of NiFeCo-LDH@MXene's overall water splitting capabilities was undertaken (Figs. 13b and c). Figs. 13d and c illustrate the HER and OER LSV profiles of various catalysts at the current density of 10 mA/cm^2. Notably, NiFeCo-LDH@MXene exhibited a minimal overpotential requirement (34 mV *vs.* RHE for HER, 130 mV *vs.* RHE for OER). These findings underscored that NiFeCo-LDH@MXene outperformed Pt/C in electrocatalytic activity and surpassed other evaluated materials in terms of lower overpotentials. Moreover, the superior performance is primarily due to the catalyst's expedited reaction kinetics, evidenced by Tafel slopes of 52 mV/dec for OER and 62 mV/dec for HER, indicative of swift electrocatalytic reaction velocities. This confirms the great potential of these catalysts for bifunctional water splitting applications.

Based on the superior electrocatalytic characteristics of NiFe-LDH@MXene and NiFeCo-LDH@MXene catalysts for both HER and OER, two-electrode devices were assembled for overall water splitting: NiFe-LDH@MXene (anode)||NiFe-LDH@MXene (cathode) and NiFeCo-LDH@MXene (anode)||NiFeCo-LDH@MXene (cathode). As shown in Fig. 13f, the NiFeCo-LDH@MXene||NiFeCo-LDH@MXene device exhibited a low cell voltage of 1.41 V to achieve a current density of 10 mA/cm^2 at a scan rate of 10 mV/s, with lower charge transfer resistance (Fig. 13g). This performance is superior to the NiFe-LDH@MXene||NiFe-LDH@MXene device (1.61 V) and the benchmark Pt/C||RuO_2 system (1.75 V). Furthermore, chronoamperometric tests were conducted on both NiFe-LDH@MXene and NiFeCo-LDH@MXene catalysts at constant cell voltages for continuous water electrolysis over 24 h (Fig. 13h). The results demonstrated the robust behavior of the prepared catalysts, maintaining stable currents without notable degradation throughout the test period. The exceptional performance of NiFeCo-LDH@MXene nanohybrids is primarily attributed to its distinctive structural and compositional attributes. The honeycomb-like porous architecture escalates the active site count and bolsters charge and mass transfer efficacy. The high conductivity and layered structure of MXene augment charge transfer efficiency, while the encapsulation of NiFeCo-LDH nanoparticles fortifies structural integrity. DFT calculations substantiated the synergistic interplay between NiFeCo-LDH and MXene, optimizing reaction kinetics and minimizing reaction barriers. Morphological analyses *via* SEM and TEM elucidated the microstructure of NiFeCo-LDH@MXene. As showcased in Fig. 13b, MXene presented a layered sheet structure, contrasted by NiFeCo-LDH@MXene's distinctive honeycomb-like porous morphology, which amplifies the electrochemical active surface area and fosters electrolyte-active site interfacing. Elemental mapping analysis affirmed the uniform dispersion of Ni, Fe, Co, Ti, C, and O elements throughout the nanohybrids. In essence, the NiFeCo-LDH@MXene has manifested high activity, rapid reaction kinetics, and stellar stability in overall water splitting, positioning it as a distinguished contender for green energy conversion technologies. This pioneering study has imparted novel perspectives on the design of high-efficiency electrocatalysts, marking a significant stride toward the progression of sustainable energy solutions.

In the cutting-edge domain of electrochemical energy conversion and storage, Han *et al.* [82] have pioneered a groundbreaking trifunctional CoS_2@MXene catalyst, marking a significant advance in electrochemical energy conversion and storage. This innovative material integrates one-dimensional (1D) CoS_2 nanowires with 2D $Ti_3C_2T_x$ MXene nanosheets through a sophisticated yet efficient synthesis process. The method involves a hydrothermal reaction followed by sulfurization, resulting in a unique hybrid nanostructure. Detailed morphological analysis using SEM and TEM reveals the catalyst's intricate architecture. SEM images (Figs. 14a and b) and TEM observations (Fig. 14c) confirm that CoS_2 nanowires are uniformly and parallelly anchored on discrete MXene nanosheets. This arrangement effectively prevents aggregation and restacking of the components, preserving the high surface area and accessibility. The strategic design of this heterostructure offers several key advantages. It significantly enhances the interface between the electrolyte and electrode, providing a wealth of reaction sites. Additionally, the unique configuration promotes efficient mass transport of reactants, a critical factor in high-performance electrochemical systems. By synergistically combining 1D and 2D nanomaterials, the CoS_2@MXene catalyst represents a new paradigm in materials design for advanced electrochemical applications. This innovative approach not only addresses current limitations in catalyst performance but also opens new avenues for the development of next-generation energy conversion and storage technologies.

The electrocatalytic performance of CoS_2@MXene, CoS_2, and MXene catalysts coated on nickel foams was evaluated for both HER and OER in 0.1 mol/L KOH solution. For HER (Fig. 14d), CoS_2@MXene nanohybrids demonstrated superior activity and faster kinetics compared to CoS_2 and MXene individually. Specifically, CoS_2@MXene achieved a lower overpotential of 175 mV at the current density of 10 mA/cm^2, outperforming CoS_2 (225 mV) and MXene (260 mV). Although its Tafel slope of 97 mV/dec was higher than that of Pt/C (36 mV/dec), suggesting a Volmer-Heyrovsky mechanism, the overall HER performance was notable. In the OER process (Fig. 14e), CoS_2@MXene exhibited exceptional performance, requiring only 270 mV overpotential to reach 10 mA/cm^2. This surpassed the performance of CoS_2 (323 mV), MXene (431 mV), and even commercial RuO_2 (302 mV). CoS_2@MXene also showed the smallest Tafel slope (92 mV/dec) among the tested catalysts, significantly lower than CoS_2 (96 mV/dec) and MXene (204 mV/dec). Furthermore, C_{dl} measurements revealed that CoS_2@MXene possessed a larger electrochemically active surface area, with a C_{dl} value of 28 mF/cm^2 (Figs. 14f and g), superior to CoS_2 (9 mF/cm^2) and MXene (2 mF/cm^2). This increased active area contributes to the enhanced catalytic performance. The exceptional HER and OER performance of CoS_2@MXene can be attributed to the synergistic effect between CoS_2 and MXene components, highlighting the effectiveness of this hybrid nanostructure in electrocatalytic applications for water splitting.

The exceptional electrochemical properties of CoS_2@MXene nanohybrids in both HER and OER were harnessed to create a highly efficient water splitting system. This innovative electrolyzer demonstrates remarkable performance, requiring only 1.63 V to achieve a current density of 10 mA/cm^2. This voltage requirement represents a significant improvement over systems utilizing either CoS_2 or MXene independently, clearly illustrating the synergistic benefits of the hybrid approach (Fig. 14h). To rigorously evaluate the system's long-term viability, an extensive durability test was conducted. The electrolyzer maintained a constant current density of 10 mA/cm^2 over a continuous 24 h water splitting operation (Fig. 14i). Notably, the potential increase remained minimal throughout this prolonged test, underscoring the exceptional stability of the CoS_2@MXene hybrid electrodes. The combination of high catalytic activity and remarkable durability positions CoS_2@MXene as a cutting-edge multifunctional catalyst for efficient water electrolysis, particularly excelling in alkaline conditions. These findings not only demonstrate the immediate practical potential of CoS_2@MXene but also highlight the broader implications of intelligently designed hybrid nanostructures in advancing electrochemical energy conversion technologies. By bridging the gap between laboratory innovation and real-world application, this research paves the way for more efficient, stable, and sustainable water splitting systems. The success of CoS_2@MXene exemplifies how strategic material design can address key challenges in renewable energy technologies, offering promising avenues for future developments in clean hydrogen production and energy storage solutions.

In recent years, single-atom catalysts have garnered significant attention due to their distinct advantages in maximizing atomic efficiency and exhibiting superior catalytic activity, showing potential for large-scale application in overall water splitting [67,68,110]. Zhang *et al.* [67] reported a single transition-metal atom anchored on the Cr_2CO_2 MXene surface as a bifunctional electrocatalyst for water splitting, investigated through DFT calculations. As a result, Ni anchored on Cr_2CO_2 (Ni/Cr_2CO_2) MXene exhibits remarkable catalytic activity, producing low overpotentials of 0.16 and 0.46 V for HER and OER, respectively. A substantial electron transfer from Ni to the surface O* of Cr_2CO_2 MXene was observed, enhancing the binding strength between Ni and Cr_2CO_2 MXene with a binding energy of −5.16 eV. The ultrahigh Ni oxide formation pressure ensures the stability of Ni/Cr_2CO_2 during electrocatalytic water splitting. Furthermore, *ab initio* molecular dynamics simulations and climbing nudged elastic band calculations suggest that the Ni atom can be stably immobilized on the Cr_2CO_2 MXene substrate, preventing its aggregation into Ni3 and Ni4 clusters. We also predict a possible synthesis route for the Cr_2CO_2-supported Ni single-atom catalyst system, indicating that Ni/Cr_2CO_2 can be experimentally synthesized. This study provides valuable insights into the design and application of single-atom catalysts for efficient water splitting, contributing to the ongoing efforts to develop sustainable energy technologies.

Peng *et al.* [68] show that in 0.1 mol/L $HClO_4$ solution, a novel single atom catalyst comprised of single ruthenium atomic sites

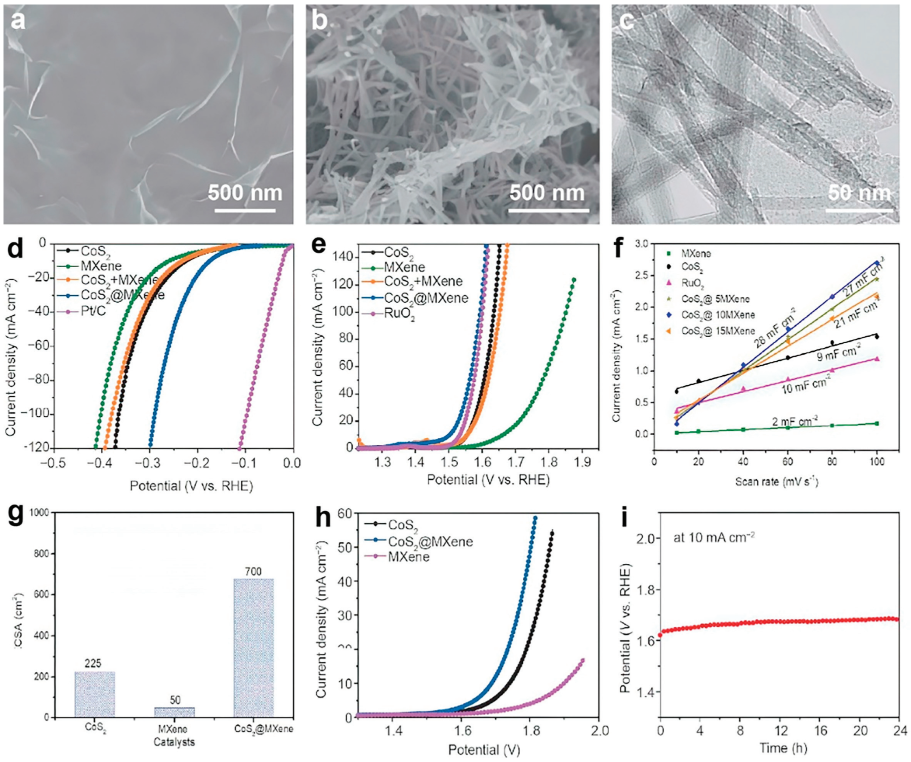

Fig. 14. (a) SEM image of $Ti_3C_2T_x$ MXene nanosheets. (b) SEM and (c) TEM images of CoS_2@MXene nanohybrids. (d) HER and (e) OER polarization curves of these various electrocatalysts. (f) ECSA of CoS_2, MXene, and CoS_2@MXene catalysts. (g) LSV curves based on the bifunctional electrodes of the various electrocatalysts towards overall water splitting. (h) The stability test at 10 mA/s of the CoS_2@MXene in the overall water splitting. (i) Overall water splitting device self-driven by two series zinc-air batteries fabricated by the CoS_2@MXene catalyst. Reproduced with permission [60]. Copyright 2020, Springer Nature.

supported on ultrathin $Ti_3C_2T_x$ MXene nanosheets (denoted as Ru-SA/$Ti_3C_2T_x$) (Figs. 15a-c), simultaneously catalyzed the HER, OER, and oxygen reduction reaction (ORR). Excitingly, Ru-SA/$Ti_3C_2T_x$ has excellent comprehensive performances. For acidic HER (Figs. 15d and e), it shows a Pt-like activity with a low overpotential (η_{10}) value at 10 mA/cm^2 of 70 mV, fast reaction kinetics (27.7 mV/dec), and high mass activity (6.62 A/mg$_{Ru}$). For acidic OER (Fig. 15f), the required η_{10} is 290 mV, which is lower than that of commercial IrO_2 (330 mV). They use the Ru-SA/$Ti_3C_2T_x$ as both anode and cathode to assess its feasibility for a two-electrode acidic electrolyzer (Fig. 15g), the current density of 10 mA/cm^2 can be obtained at a small cell voltage of 1.56 V (Fig. 15h), which is 190 mV less than that required for the Pt/C||IrO_2 couple and among the best values published for acidic overall water splitting. In addition to the high efficiency and durability for HER and OER (Fig. 15i), Ru-SA/$Ti_3C_2T_x$ also exhibits superior acidic ORR performance with a positive half-wave potential of 0.80 V *vs.* RHE, the highest kinetic current density of −4.98 mA/cm^2 at 0.8 V *vs.* RHE, and a Tafel slope of 60.4 mV/dec which are record-level among previously reported ORR catalysts. Further, when the Ru-SA/$Ti_3C_2T_x$ was applied in a proton exchange membrane fuel cell as a cathode catalyst, the maximum power density was found to be 941 mW/cm^2, exceeding most of the best-reported precious/transition metal catalysts. Before this work, no SA catalysts could provide simultaneously high activity and good stability for the acidic HER, OER, and ORR. Furthermore, experiments and DFT calculations clearly reveal that the two-fold O-coordinated configuration of each Ru site can optimize the adsorption of reactants/intermediates, making HER, OER, and ORR pathways on the designed catalyst along an energetic-favorable process. This synergistic effect between the MXene support and the precisely positioned single-atom catalysts opens up new avenues for designing high-performance, earth-abundant electrocatalysts for clean energy applications. This study not only advances our understanding of single-atom catalysis but also provides a promising pathway for the development of efficient and durable catalysts for hydrogen production.

Rogach *et al.* [110] conducted a comprehensive investigation into the intricate electronic architecture and remarkable electrocatalytic prowess of nanohybrids crafted by strategically anchoring Co single atoms onto distinct MXene substrates: V_2CT_x, Nb_2CT_x, and $Ti_3C_2T_x$, *via* an ingenious photochemical reduction approach (Fig. 16a). This innovative strategy harnessed the unparalleled strength of hybridization interactions between the Co 3d orbitals and the surface-terminated O 2p orbitals in the Co@V_2CT_x nanohybrids, fostering a pronounced electron transfer from Co to the V_2CT_x matrix. Remarkably, when benchmarked against its counterparts, Co@V_2CT_x exhibited superior electrochemical performance, manifesting in notably reduced overpotentials for both OER and HER, at 242 mV and 35 mV respectively, at a current density of 10 mA/cm^2 in 1.0 mol/L KOH electrolyte (Figs. 16b and c). This outstanding performance underscores the exceptional catalytic efficiency of Co@V_2CT_x.

To delve deeper into the underlying mechanisms of this enhanced electrocatalytic behavior, a meticulous analysis was conducted, encompassing the calculation of Gibbs free energies for each step in the OER and HER pathways, the projected density of states (PDOS), and the Bader charges (Figs. 16d-f). These insights revealed that the reduced Gibbs free energy variation for the rate-limiting step in the OER pathway of Co@V_2CT_x (1.78 eV), compared to Co@Nb_2CT_x (1.91 eV) and Co@$Ti_3C_2T_x$ (2.49 eV), facilitated a more favorable transformation from *O to *OOH, indicative of an accelerated OER kinetics. Similarly, the lower Gibbs free energy of hydrogen adsorption in Co@V_2CT_x (0.31 eV), as opposed to Co@Nb_2CT_x (0.38 eV) and Co@$Ti_3C_2T_x$ (0.43 eV), hinted at a more efficient formation and subsequent release of molecular hydrogen, thereby enhancing the HER performance.

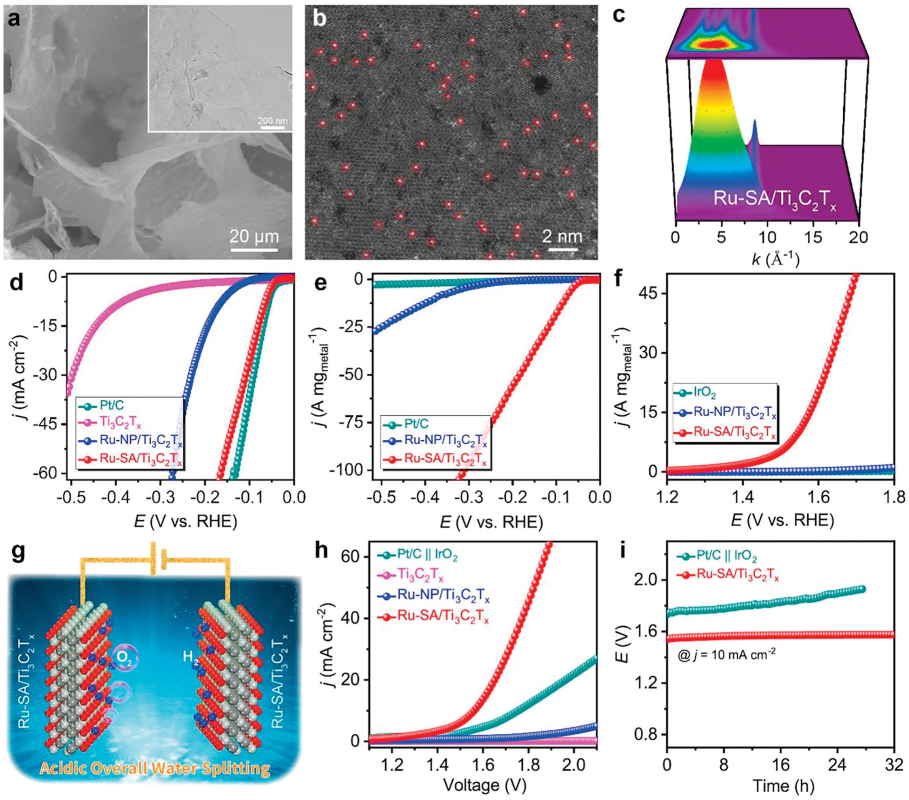

Fig. 15. (a) Low-magnification SEM image of Ru-SA/$Ti_3C_2T_x$. (b) Aberration-corrected HAADF-STEM image of Ru-SA/$Ti_3C_2T_x$. (c) WT-EXAFS plot of Ru-SA/$Ti_3C_2T_x$. (d) Geometric-area-normalized HER curves. (e) The corresponding Ru-mass-loading-normalized HER curves. (f) Geometric-area-normalized OER curves. (g) Schematic of Ru-SA/$Ti_3C_2T_x$ as bifunctional electrocatalysts for OER and HER in a 0.1 mol/L $HClO_4$ solution. (h) Geometric-area-normalized overall water splitting LSV curves. (i) Stability test. Reproduced with permission [68]. Copyright 2020, Wiley.

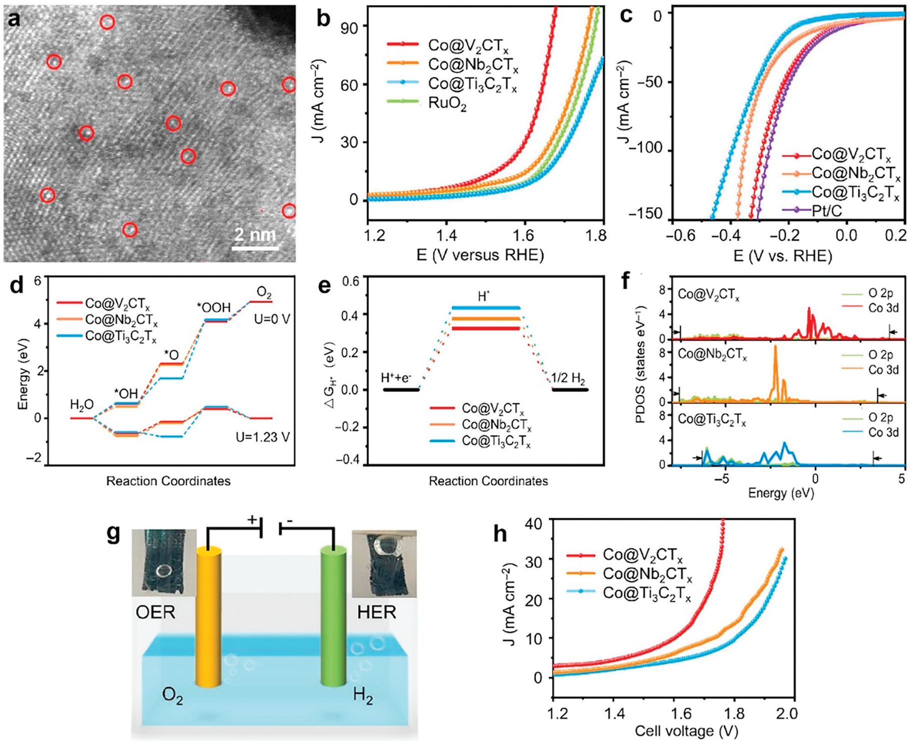

Fig. 16. (a) HAADF-STEM image of the surface of Co@V_2CT_x. (b) OER and (c) HER LSV curves at a scan rate of 5 mV/s. (d) Calculated OER free energy diagrams. (e) Calculated HER Gibbs free energies. (f) Calculated PDOS of the Co d-band and O p-band. (g) Illustration of the overall water splitting device. (h) LSV polarization curves of three bifunctional electrodes in 1.0 mol/L KOH for overall water splitting. Reproduced with permission [110]. Copyright 2023, Wiley.

Furthermore, the deployment of Co@V_2CT_x as a bifunctional catalyst, serving both as the cathode and anode in a water splitting electrolyzer, showcased remarkable stability over an extended duration of 10 h with minimal degradation, operating at a commendably low potential of 1.60 V (Figs. 16g and h). This underscores its potential for practical applications requiring sustained and efficient electrochemical water splitting. In conclusion, the study underscores the pivotal role of MXene substrates, particularly V_2CT_x, in amplifying the electrocatalytic properties of cobalt single-atom catalysts, offering promising avenues for the development of highly efficient and durable electrocatalysts for renewable energy conversion technologies.

7. Summary and outlook

MXene-derived materials have emerged as versatile electrocatalysts for water electrolysis, capable of facilitating both HER and OER at the cathode and anode, respectively. This dual functionality, combined with their renewable nature and eco-friendly characteristics, positions MXene-derived materials as a promising solution to address the global energy crisis and mitigate environmental pollution associated with traditional hydrogen production methods. The potential for a truly sustainable hydrogen production process becomes evident when these catalysts are coupled with renewable energy sources like solar and wind power, and synthesized using environmentally benign methods such as molten salt etching or electrochemical etching. Under these conditions, and assuming technological maturity and cost-effectiveness, MXene-based catalysts can enable water electrolysis with minimal environmental impact. The resulting "green hydrogen" offers significant advantages, including high energy density and zero-emission combustion, making it a compelling clean energy alternative to fossil fuels. Moreover, its application in ammonia synthesis and fuel cells has the potential to substantially reduce carbon emissions in the chemical industry and contribute to greenhouse gas mitigation efforts. As research and development in this field progress, MXene-based catalysts are expected to play a crucial role in advancing sustainable hydrogen production technologies, thereby making substantial contributions to environmental conservation and the transition towards a cleaner, more sustainable energy landscape.

The catalytic efficacy of MXenes is fundamentally determined by two key factors: The abundance of active sites and their intrinsic reactivity. Enhancing the electrocatalytic performance of these materials can be achieved through two primary strategies: Increasing the number of active sites, such as edges and atomic vacancies, or amplifying the inherent activity of existing sites through functional group modification, material hybridization, or elemental doping. This review comprehensively examines the catalytic applications of MXene materials in HER, OER, and overall water splitting, focusing on both precious and non-noble metal systems. MXenes demonstrate remarkable versatility in their catalytic applications, serving in three distinct capacities: as direct catalysts, as foundational materials for other catalytic substances to enhance overall catalytic effects, and in combination with single-function catalytic materials through processes like encapsulation, fusion, and coupling to produce bifunctional catalysts. This multifaceted approach to utilizing MXenes in electrocatalysis underscores their potential to revolutionize the field of water splitting and contribute significantly to the development of more efficient and sustainable energy technologies.

MXenes have emerged as exceptionally promising materials for electrocatalysis, yet current research remains largely confined to a few early-group MXenes, particularly $Ti_3C_2T_x$, with limited exploration of their catalytic mechanisms. To fully harness the potential of these materials, future research must address several critical challenges: expanding the scope of MXene materials under investigation, overcoming limitations in nitride MXene studies, elucidating theoretical catalytic mechanisms for MXene-based catalysts, and developing a comprehensive framework to guide the creation of novel, highly efficient MXene-based catalysts. A recent breakthrough in this field, the integration of transition metal (oxide) hydroxides with MXenes for alkaline HER, demonstrating Pt-like electrocatalytic performance, has challenged the long-held belief that transition metal oxides exhibit poor electrocatalytic activity under alkaline conditions. This milestone not only opens new avenues for MXene-based catalyst research but also emphasizes the importance of challenging conventional wisdom and embracing innovative thinking.

Moreover, the frontier of MXene-based nanohybrids is poised to revolutionize metal-air battery technology, particularly for lithium-air and Zn-air battery systems, offering a paradigm shift in energy storage solutions. These materials, characterized by their exceptional electrical conductivity, vast surface area, and highly tunable surface chemistry, stand at the vanguard of next-generation energy systems. However, the full potential of these innovative materials remains constrained by the sluggish kinetics of ORR and OER at the air cathode. To surmount these challenges, future research must embark on a multifaceted approach to catalytic activity optimization. This endeavor may encompass strategic transition metal doping, the synthesis of synergistic hybrid nanostructures, and the precise engineering of single-atom catalysts on MXene surfaces. Concurrently, elucidating and enhancing the long-term stability of these materials in the harsh, oxidizing environments typical of metal-air batteries is paramount. Successfully navigating these research avenues could yield transformative advancements in energy density, power output, and cycle life, with profound implications for portable electronics, electric vehicles, and grid-scale energy storage. Such breakthroughs would not only accelerate the global transition to clean energy technologies but also provide invaluable insights applicable to a broader spectrum of electrochemical systems, including fuel cells and electrolyzers. As this field matures, it is imperative to adopt a holistic research paradigm that balances performance optimization with scalability, cost-effectiveness, and environmental sustainability. Furthermore, integrating these materials into practical devices and scaling up production processes will be crucial steps toward realizing their full potential. By addressing these multifaceted challenges, MXene-based nanohybrids could play a pivotal role in sculpting a sustainable energy landscape, significantly contributing to climate change mitigation and the realization of a carbon-neutral future. This research trajectory not only promises to redefine the boundaries of energy storage technology but also exemplifies the critical role of materials science in addressing global environmental challenges.

Declaration of competing interest

The authors declare that they have no known competing financial interests or personal relationships that could have appeared to influence the work reported in this paper.

CRediT authorship contribution statement

Liwei Hou: Writing – original draft, Data curation, Conceptualization. **Xianyun Peng:** Writing – review & editing, Supervision, Project administration, Funding acquisition, Conceptualization. **Siliu Lyu:** Writing – original draft. **Zhongjian Li:** Writing – original draft, Supervision. **Bin Yang:** Writing – original draft, Supervision. **Qinghua Zhang:** Writing – original draft. **Qinggang He:** Visualization, Data curation. **Lecheng Lei:** Investigation, Data curation. **Yang Hou:** Writing – review & editing, Supervision, Project administration, Funding acquisition.

Acknowledgments

The authors are grateful financial support from the National Natural Science Foundation of China (Nos. 22278364, 22208296, U22A20432, 22211530045, 22178308, 22208076), the development project of Zhejiang Province's "Jianbing" and "Lingyan" (No. 2023C01226), Science Foundation of Donghai Laboratory (No. DH-2022ZY0009), National Key Research and Development Program of China (No. 2022YFB4002100), the Zhejiang Province Basic Public Welfare Research Program (Nos. LQ24B030007, LQ23B060001), the Fundamental Research Funds for the Central Universities (Nos. 226–2022–00044, 226–2024–00060), the Research Funds of Institute of Zhejiang University-Quzhou (Nos. IZQ2021RCZX026, IZQ2021KJ2008), Key Technology Breakthrough Program of Ningbo "Science and Innovation Yongjiang 2035" (No. 2024H024), the Hubei Provincial Natural Science Foundation of China (No. 2024AFB1036), the Doctoral Scientific Research Foundation of Hubei University of Automotive Technology (No. BK202354).

References

[1] T.Y. Shuai, Q.N. Zhan, H.M. Xu, et al., Green Chem. 25 (2023) 1749–1789.
[2] K. Liu, H. Yang, Y. Jiang, et al., Nat. Commun. 14 (2023) 2424.
[3] Y.J. Lei, Z.C. Yan, W.H. Lai, et al., Electrochem. Energy Rev. 3 (2020) 766–792.
[4] H.T. Das, T.E. Balaji, S. Dutta, et al., Int. J. Energ. Res. 46 (2022) 8625–8656.
[5] X. Bai, J. Guan, Chin. J. Catal. 43 (2022) 2057–2090.
[6] I. Dincer, C. Zamfirescu, Int. J. Hydrogen Energ. 37 (2012) 16266–16286.
[7] S. Anantharaj, S. Noda, Small 16 (2019) 1905779.
[8] M. Khan, A. Hussain, M.T. Saleh, et al., Coordin. Chem. Rev. 506 (2024) 215722.
[9] H. Liang, J. Liu, ChemCatChem 14 (2022) e202101375.
[10] B. You, M.T. Tang, C. Tsai, et al., Adv. Mater. 31 (2019) e1807001.
[11] D. Guo, Q. Pan, T. Vietor, et al., J. Energ. Chem. 87 (2023) 518–539.
[12] J. Ran, J. Zhang, J. Yu, et al., Chem. Soc. Rev. 43 (2014) 7787–7812.
[13] B. You, Y. Sun, Acc. Chem. Res. 51 (2018) 1571–1580.
[14] N. Danilovic, R. Subbaraman, K.C. Chang, et al., Angew. Chem. Int. Ed. 53 (2014) 14016–14021.
[15] J. Yoon, J. Park, Y.J. Sa, et al., CrystEngComm 18 (2016) 6002–6007.
[16] L. Yang, M.B. Vukmirovic, D.K. Su, et al., J. Phys. Chem. C 117 (2013) 1748–1753.
[17] M.K. Debe, Nature 486 (2012) 43–51.
[18] H.A. Gasteiger, S.S. Kocha, B. Sompalli, et al., Appl. Catal. B: Environ. 56 (2005) 9–35.
[19] M. Khan, N. Shahzad, C. Xiong, et al., Diam. Relat. Mater. 61 (2016) 32–40.
[20] M. Khan, A.A. Khurram, L. Tiehu, et al., Diam. Relat. Mater. 78 (2017) 58–66.
[21] M.R. Lukatskaya, O. Mashtalir, C.E. Ren, et al., Science 341 (2013) 1502–1505.
[22] M. Naguib, M. Kurtoglu, V. Presser, et al., Adv. Mater. 23 (2011) 4248–4253.
[23] Y. Tong, P. Chen, L. Chen, et al., ChemSusChem 14 (2021) 2576–2584.
[24] M. Naguib, J. Halim, J. Lu, et al., J. Am. Chem. Soc. 135 (2013) 15966–15969.
[25] X. Sang, Y. Xie, M.W. Lin, et al., ACS Nano 10 (2016) 9193–9200.
[26] Y. Gogotsi, B. Anasori, ACS Nano 13 (2019) 8491–8494.
[27] Y.J. Kim, S.J. Kim, D. Seo, et al., Chem. Mater. 33 (2021) 6346–6355.
[28] A. Alarawi, V. Ramalingam, J.H. He, Mater. Today Chem. 11 (2019) 1–23.
[29] G.H. Jeong, S.P. Sasikala, T. Yun, et al., Adv. Mater. 32 (2020) 1907006.
[30] X. Li, Z. Huang, C. Zhi, Front. Mater. 6 (2019) 312.
[31] T.Y. Shuai, Q.N. Zhan, H.M. Xu, et al., Chem. Commun. 59 (2023) 3968–3999.
[32] C.E. Shuck, Y. Gogotsi, Chem. Eng. J. 401 (2020) 125786.
[33] B. Anasori, M.R. Lukatskaya, Y. Gogotsi, Nat. Rev. Mater. 2 (2017) 16098.
[34] B.M. Jun, S. Kim, J. Heo, et al., Nano Res. 12 (2018) 471–487.
[35] Y. Sun, Y. Li, Chemosphere 271 (2021) 129578.
[36] L. Chen, M. Wakeel, T. Ul Haq, et al., Environ. Sci. Nano 9 (2022) 3168–3205.
[37] I. Ashraf, S. Ahmad, F. Nazir, et al., Int. J. Hydrogen Energ. 47 (2022) 27383–27396.
[38] Y. Wu, W. Wei, R. Yu, et al., Adv. Funct. Mater. 32 (2022) 2110910.
[39] Y. Jiang, T. Sun, X. Xie, et al., ChemSusChem 12 (2019) 1368–1373.
[40] A. Patra, R. Samal, C.S. Rout, Catal. Today 424 (2023) 113853.
[41] L.P. Hao, A. Hanan, R. Walvekar, et al., Catalysts 13 (2023) 802.
[42] Z. Lv, W. Ma, M. Wang, et al., Adv. Funct. Mater. 31 (2021) 2102576.
[43] A. Hanan, M.N. Lakhan, M.Y. Solangi, et al., Mater. Today Sustain. 24 (2023) 100585.
[44] B. Zhang, J. Shan, X. Wang, et al., Small 18 (2022) 2200173.
[45] Y. Xu, Z. Mao, J. Zhang, et al., Angew. Chem. Int. Ed. (63) (2024) e202316029.
[46] A.Gilbert Prince, L. Durai, S. Badhulika, FlatChem 36 (2022) 100439.
[47] Y. Ye, X. Zeng, Y. Wang, et al., J. Adv. Ceram. 12 (2023) 553–564.
[48] S.K. Raj, V.Sharma Kirti, et al., Int. J. Hydrogen Energ. 48 (2023) 37732–37745.
[49] K. Chaudhary, S. Zulfiqar, H.H. Somaily, et al., Electrochim. Acta 431 (2022) 141103.
[50] M. Li, S. Zhou, R. Sun, et al., Fuel 358 (2024) 130256.
[51] X. Yu, L. Lin, C. Pei, et al., Chemistry 30 (2023) e202303524.
[52] X. Shi, M. Du, H.S. Jing, et al., Colloids Surf. A 679 (2023) 132638.
[53] M. Xu, J. Huang, X. Yue, et al., ACS Appl. Energ. Mater. 7 (2024) 2460–2468.
[54] N. Li, Y. Zhang, M. Jia, et al., Electrochimica. Acta 326 (2019) 134976.
[55] X. Li, X. Lv, X. Sun, et al., App. Catal. B: Environ. 284 (2021) 119708.
[56] C.F. Du, Q. Song, Q. Liang, et al., ChemNanoMat 7 (2021) 539–544.
[57] X. Zhao, W.P. Li, Y. Cao, et al., ACS Nano 18 (2024) 4256–4268.
[58] V. Ramalingam, P. Varadhan, H.C. Fu, et al., Adv. Mater. 31 (2019) e1903841.
[59] S. Hussain, D. Vikraman, G. Nazir, et al., Nanomaterials 12 (2022) 2886.
[60] S. Han, Y. Chen, Y. Hao, et al., China Mater. 64 (2020) 1127–1138.
[61] X. Peng, Y. Mi, X. Liu, et al., J. Mater. Chem. A 10 (2022) 6134–6145.
[62] X. Peng, H. Bao, J. Sun, et al., Nanoscale 13 (2021) 7134–7139.
[63] J. Zhang, E. Wang, S. Cui, et al., Nano Lett. 22 (2022) 1398–1405.
[64] W. Lin, Y.R. Lu, W. Peng, et al., J. Mater. Chem. A 10 (2022) 9878–9885.
[65] A.Gilbert Prince, L. Durai, S. Badhulika, FlatChem 36 (2022) 100439.
[66] X. Zeng, Y. Ye, Y. Wang, et al., J. Adv. Ceram. 12 (2023) 553–564.
[67] Y. Cheng, J. Dai, Y. Song, et al., ACS App. Energ. Mater. 2 (2019) 6851–6859.
[68] X. Peng, S. Zhao, Y. Mi, et al., Small 16 (2020) e2002888.
[69] C.G. Morales-Guio, L.A. Stern, X. Hu, Chem. Soc. Rev. 43 (2014) 6555–6569.
[70] Y. Yan, B.Y. Xia, B. Zhao, et al., J. Mater. Chem. A 4 (2016) 17587–17603.
[71] N.T. Suen, S.F. Hung, Q. Quan, et al., Chem. Soc. Rev. 46 (2017) 337–365.
[72] I.C. Man, H.Y. Su, F. Calle-Vallejo, et al., ChemCatChem 3 (2011) 1159–1165.
[73] J. Zhang, H.B. Yang, D. Zhou, B. Liu, Chem. Rev. 122 (2022) 17028–17072.
[74] C. Lei, S. Lyu, J. Si, et al., ChemCatChem 11 (2019) 5855–5874.
[75] M. Gao, F. Wang, S. Yang, et al., Mater. Today 72 (2024) 318–358.
[76] X. Li, Z. Huang, C.E. Shuck, et al., Nat. Rev. Chem. 6 (2022) 389–404.
[77] J. Björk, J. Halim, J. Zhou, et al., npj 2D Mater. Appl. 7 (2023) 5.
[78] Y. Wei, P. Zhang, R.A. Soomro, et al., Adv. Mater. 33 (2021) e2103148.
[79] M. Han, K. Maleski, C.E. Shuck, et al., J. Am. Chem. Soc. 142 (2020) 19110–19118.
[80] B. Anasori, Y. Xie, M. Beidaghi, et al., ACS Nano 9 (2015) 9507–9516.
[81] Q. Tao, M. Dahlqvist, J. Lu, et al., Nat. Commun. 8 (2017) 14949.
[82] M. Shekhirev, C.E. Shuck, A. Sarycheva, et al., Prog. Mater. Sci. 120 (2021) 100757.
[83] V. Kamysbayev, A.S. Filatov, H. Hu, et al., Science 369 (2020) 979–983.
[84] Y. Li, H. Shao, Z. Lin, et al., Nat. Mater. 19 (2020) 894–899.
[85] S.G. Peera, R. Koutavarapu, L. Chao, et al., Micromachines 13 (2022) 1499.
[86] R. Verma, A. Sharma, V. Dutta, et al., Emergent Mater. 7 (2023) 35–62.
[87] Z. Kang, M.A. Khan, Y. Gong, et al., J. Mater. Chem. A 9 (2021) 6089–6108.
[88] R.R. Raja Sulaiman, A. Hanan, W.Y. Wong, et al., Catalysts 12 (2022) 1576.
[89] Y. Wen, Z. Wei, C. Ma, et al., Nanomaterials 9 (2019) 775.
[90] Y. Jiang, X. Wu, Y. Yan, et al., Small 15 (2019) 1805474.
[91] L. Zhang, D. Ye, Q.A. Huang, et al., J. Electrochem. Soc. 167 (2020) 1–14.
[92] Y. Zheng, Y. Liu, X. Guo, et al., J. Mater. Sci. Technol. 41 (2020) 117–126.
[93] V. Ramalingam, P. Varadhan, H.C. Fu, et al., Adv. Mater. 31 (2019) 1903841.
[94] B. Abdollahi, A. Najafidoust, E.Abbasi Asl, et al., Arabian J. Chem. 14 (2021) 103444.
[95] A. Hanan, M.N. Lakhan, M.Y. Solangi, et al., Mater. Today Sustain. 24 (2023) 100585.
[96] Y. Yang, X. Huang, C. Sheng, et al., J. Alloys Compd. 920 (2022) 165908.
[97] Y. Tang, C. Yang, M. Sheng, et al., ACS Sustain. Chem. Eng. 8 (2020) 12990–12998.
[98] C.F. Du, X. Sun, H. Yu, et al., Adv. Sci. 6 (2019) 1900116.
[99] K. Wang, H. Du, S. He, et al., Adv. Mater. 33 (2021) 2005587.
[100] X. Zheng, X. Han, Y. Cao, et al., Adv. Mater. 32 (2020) 2000607.
[101] J. Li, C. Chen, Z. Lv, et al., J. Mater. Sci. Technol. 145 (2023) 74–82.
[102] S. Zhao, Y. Wang, J. Dong, et al., Nat. Energ. 1 (2016) 16184.
[103] M.S. Burke, M.G. Kast, L. Trotochaud, et al., J. Am. Chem. Soc. 137 (2015) 3638–3648.
[104] Y. Pan, R. Lin, Y. Chen, et al., J. Am. Chem. Soc. 140 (2018) 4218–4221.
[105] L. Cao, Q. Luo, W. Liu, et al., Nat. Catal. 2 (2019) 134–141.
[106] Z. Chen, X. Fan, Z. Shen, et al., ChemCatChem 12 (2020) 4059–4066.
[107] Z. Fu, G. Hai, X.X. Ma, et al., J. Energ. Chem. 98 (2024) 663–669.
[108] H. Su, S. Song, S. Li, et al., App. Catal. B: Environ. 293 (2021) 120225.
[109] L. Zhang, Y. Jia, G. Gao, et al., Chem 4 (2018) 285–297.
[110] X. Zhao, X. Zheng, Q. Lu, et al., EcoMat 5 (2023) e12293.